Bleier, N.; Mosler, J.:

Efficient variational constitutive updates by means of a novel parameterization of the flow rule

In: International Journal for Numerical Methods in Engineering (2011) Wiley

DOI: 10.1002/nme.3280

Efficient variational constitutive updates by means of a novel parameterization of the flow rule

N. Bleier

Institute of Mechanics
Ruhr University Bochum
D-44780 Bochum, Germany

J. Mosler

Materials Mechanics
Institute of Materials Research
Helmholtz-Zentrum Geesthacht
D-21502 Geesthacht, Germany
E-Mail: joern.mosler@hzg.de

SUMMARY

Analogously to the classical return-mapping algorithm, so-called *variational constitutive updates* are numerical methods allowing to compute the unknown state variables such as the plastic strains and the stresses for material models showing an irreversible mechanical response. In sharp contrast to standard approaches in computational inelasticity, the state variables follow naturally and jointly from energy minimization in case of variational constitutive updates. This leads to significant advantages from a numerical, mathematical as well as from a physical point of view. However, while the classical return-mapping algorithm has been being developed for several decades and thus, it has already reached a certain maturity, variational constitutive updates have drawn attention only relatively recently. This is particularly manifested in the numerical performance of such algorithms. Within the present paper, the numerical efficiency of variational constitutive updates is critically analyzed. It will be shown that a naive approximation of the flow rule causes a singular Hessian within the respective Newton-Raphson scheme. However, by developing a novel parameterization of the flow rule, an efficient algorithm is derived. Its performance is carefully compared to that of the classical return-mapping scheme. This comparison clearly shows that the novel variationally consistent implementation is, at least, as efficient as the classical return-mapping algorithm.

1 Introduction

For constitutive models capturing dissipative mechanisms, stress update algorithms are always required. Considering a strain-driven process such as that in typical finite elements based on an interpolation of the deformation mapping, the goal of such update algorithms is the computation of the state variables at time t_{n+1} by means of the internal variables at time t_n and the current strain tensor. An overview of stress update algorithms can be found in [1, 2] and in the references cited therein. Nowadays, the most frequently applied implementations are those relying on the return-mapping scheme. Within these operator-split schemes, the evolution equations and the flow rule are discretized by a backward Euler time integration and the unknowns such as the plastic strain increment are computed by solving a set of nonlinear equations. Typically, a standard Newton-Raphson iteration is employed for that purpose. Since the classical return-mapping algorithm has been being developed for several decades, it has already reached a certain maturity and has also been reasonably well understood, cf. [1, 2].

According to the previous paragraph, the return-mapping scheme is a purely mathematical technique which can be applied to other stiff nonlinear differential equations as well. Certainly, this broad range of application makes the return-mapping scheme very appealing. However, the broad range of application implies that many physically relevant principles are completely ignored within this algorithm. One such principle is that of energy stability. By way of contrast, an alternative, variationally consistent method was proposed by Ortiz and co-workers, see [3, 4]. It is based on minimizing the stress power and thus, it shares some similarities to the postulate of maximum dissipation, cf. [5, 6]. Due to the underlying variational basis, such models are referred to as *variational constitutive updates*, cf. [7–10].

Compared to conventional stress update algorithms such as the classical return-mapping scheme, variational constitutive updates show several significant advantages from a numerical and mathematical as well as from a physical point of view. Concerning a numerical and mathematical viewpoint, the probably most important feature of variational constitutive updates is that they provide an unambiguous comparison criterion for numerical solutions, cf. [11]. More specifically, solution one is better than solution two, if and only if the stress power associated with solution one is lower. This natural pseudo

metric can be used for deriving physically sound error estimates and indicators which can be employed in adaptive finite element methods (see [12–15]). From a physical point of view, the interpretation of the solution as an energy minimizer is worth mentioning. Furthermore, energy principles provide a physically sound basis for coupling different constitutive models, i.e., the energetically most favorable combination between the respective models is considered, cf. [16–18].

In spite of the aforementioned advantages, variational constitutive updates are comparably infrequently applied. The return-mapping scheme remains to be the common choice for stress update algorithms. There are, at least, two reasons associated with this.
First, most of the existing implementations for variational constitutive updates have been specifically designed for certain, relatively simple, material models, although the underlying framework itself is very general, cf. [3, 4, 7–9]. More precisely, focus is either on isotropic von Mises plasticity or on crystal plasticity theory within the cited papers. Furthermore, no general implementation exists which can be easily applied to a broad range of applications. By way of contrast, such algorithms are well-established in case of the return-mapping scheme, see [1, 2]. First ideas for a more general framework for variational constitutive updates are discussed in [10].
The second reason why variational constitutive updates have not been frequently applied yet is related to their numerical efficiency. While the classical return-mapping algorithm has already reached a certain maturity and thus, its numerical implementation has been highly optimized, the implementation of variational constitutive updates has drawn attention only relatively recently, cf. [6, 10, 18, 19].

Within the present paper, a new implementation for variational consistent updates is discussed. This implementation can be applied to a broad range of different constitutive models. In contrast to previous works on such update scheme, focus is particularly on the accuracy, numerical robustness and efficiency of the respective algorithm. As shown by numerical experiments, the resulting numerical formulation is as efficient as the return-mapping scheme – and in many cases, even more efficient. Furthermore, its range of application is very broad. For fully isotropic models (elastic energy as well as the yield function) an adapted version of this algorithm is also discussed based on a description in eigenvalues. In this connection, the underlying nonlinear set of equations shows a reduced complexity compared to a return-mapping algorithm formulated in principal stress space, cf. [1, 2].

The nonlinear set of equations describing the novel variational consistent update is solved by employing a Newton-Raphson iteration. In this connection, it is shown that a naive approximation of the flow rule causes a singular Hessian. Such numerical problems are effectively solved by a new parameterization based on pseudo stresses.

The paper is organized as follows: First the fundamentals of finite strain plasticity are introduced in Section 2.1. Subsequently, a variationally consistent reformulation of finite strain plasticity is presented in Section 3. The resulting framework, also known as variational constitutive updates, allows computing all state variables by minimizing the stress power of the respective solid. Such update schemes depend crucially on the parameterization of the flow rule. For this reason, different existing concepts are critically analyzed and further elaborated in Subsection 4. It is shown that the most general among those parameterization leads to a highly ill-conditioned Hessian matrix causing numerical problems. Consequently, an extended formulation is required. Such a formulation is elaborated in Subsection 5. Its efficiency, accuracy as well as its numerical robustness are critically analyzed in Section 6.

2 Finite strain plasticity theory in a nutshell

This section is concerned with the fundamentals of finite strain plasticity theory. The section serves mostly for introducing the notations used in the remaining part of the paper. Throughout this work, isothermal conditions are considered.

2.1 Fundamentals

Following [20], the gradient of the deformation mapping $\boldsymbol{\varphi}$, denoted as $\boldsymbol{F} := \mathrm{GRAD}\boldsymbol{\varphi}$, is multiplicatively decomposed into an elastic part $\boldsymbol{F}^{\mathrm{e}}$ and a plastic part $\boldsymbol{F}^{\mathrm{p}}$, i.e.

$$\boldsymbol{F} = \boldsymbol{F}^{\mathrm{e}} \cdot \boldsymbol{F}^{\mathrm{p}}, \qquad \text{with} \qquad \det \boldsymbol{F}^{\mathrm{e}} > 0,\ \det \boldsymbol{F}^{\mathrm{p}} > 0. \tag{1}$$

This split allows describing the elastic as well as the elastoplastic response of a solid. For that purpose, the Helmholtz energy is defined. For elastoplastic processes, an additive decomposition of this energy of the type

$$\Psi = \Psi^{\mathrm{e}}(\boldsymbol{F}^{\mathrm{e}}) + \Psi^{\mathrm{p}}(\boldsymbol{\alpha}) \tag{2}$$

represents a suitable choice, cf. [2, 21]. In Eq. (2), $\boldsymbol{\alpha} \in \mathbb{R}^n$ is a strain-like internal variable (or a suitable set) related to plastic hardening and Ψ^{p} denotes the associated stored energy. Energy due to a distortion of the underlying atomic lattice is considered by Ψ^{e}.

Based on Eq. (2), the stress-strain response implied by the model can be computed. Therefor, the by now standard Coleman & Noll procedure [22, 23] is employed. Combining the dissipation inequality

$$\mathcal{D} = \boldsymbol{P} : \dot{\boldsymbol{F}} - \dot{\Psi} \geq 0 \tag{3}$$

with Eq. (1) and Eq. (2), the second law of thermodynamics reads

$$\mathcal{D} = \left(\boldsymbol{F}^{\mathrm{p}} \cdot \boldsymbol{S} \cdot \boldsymbol{F}^{\mathrm{p}^T} - 2 \, \frac{\partial \Psi}{\partial \boldsymbol{C}^{\mathrm{e}}} \right) : \frac{1}{2} \, \dot{\boldsymbol{C}}^{\mathrm{e}} + \boldsymbol{S} : \left(\boldsymbol{F}^{\mathrm{p}^T} \cdot \boldsymbol{C}^{\mathrm{e}} \cdot \dot{\boldsymbol{F}}^{\mathrm{p}} \right) + \boldsymbol{Q} \cdot \dot{\boldsymbol{\alpha}} \geq 0. \tag{4}$$

Here and henceforth, $\boldsymbol{C}^{\mathrm{e}} := \boldsymbol{F}^{\mathrm{e}^T} \cdot \boldsymbol{F}^{\mathrm{e}}$ is the elastic right Cauchy-Green strain tensor, $\boldsymbol{P} := \partial_{\boldsymbol{F}} \Psi$ and $\boldsymbol{S} := \boldsymbol{F}^{-1} \cdot \boldsymbol{P}$ are the first and the second Piola-Kirchhoff stress tensors, $\boldsymbol{Q} := -\partial_{\boldsymbol{\alpha}} \Psi$ is a stress-like internal variable work conjugate to $\boldsymbol{\alpha}$ and the superposed dot denotes the material time derivative. Evaluating Ineq. (4) for reversible processes yields

$$\boldsymbol{S} = 2 \, \frac{\partial \Psi}{\partial \boldsymbol{C}} = 2 \, \boldsymbol{F}^{\mathrm{p}^{-1}} \cdot \frac{\partial \Psi}{\partial \boldsymbol{C}^{\mathrm{e}}} \cdot \boldsymbol{F}^{\mathrm{p}^{-T}} \tag{5}$$

and the reduced dissipation inequality

$$\mathcal{D} = \boldsymbol{\Sigma} : \boldsymbol{L}^{\mathrm{p}} + \boldsymbol{Q} \cdot \dot{\boldsymbol{\alpha}} \geq 0. \tag{6}$$

In Eq. (6), $\boldsymbol{\Sigma} = 2 \, \boldsymbol{C}^{\mathrm{e}} \cdot \partial_{\boldsymbol{C}^{\mathrm{e}}} \Psi$ is the Mandel stress tensor (cf. [24]) and $\boldsymbol{L}^{\mathrm{p}} = \dot{\boldsymbol{F}}^{\mathrm{p}} \cdot \boldsymbol{F}^{\mathrm{p}^{-1}}$ is the plastic velocity gradient.

While Eq. (5) defines the stress-strain response of the model, its evolution equations ($\boldsymbol{L}^{\mathrm{p}}$ and $\dot{\boldsymbol{\alpha}}$) remain to be specified. For that purpose, the space of admissible stresses $\mathbb{E}_{\boldsymbol{\sigma}}$ is introduced. Analogously to the reduced dissipation inequality (6), this space is formulated in terms of $\boldsymbol{\Sigma}$ and $\boldsymbol{Q}$, i.e.,

$$\mathbb{E}_{\boldsymbol{\sigma}} = \left\{ (\boldsymbol{\Sigma}, \boldsymbol{Q}) \in \mathbb{R}^{9+n} \;\middle|\; \phi(\boldsymbol{\Sigma}, \boldsymbol{Q}) \leq 0 \right\}. \tag{7}$$

Here, ϕ is the yield function which has to fulfill certain regularity conditions, cf. [25]. Now, evolution equations can be derived. In this connection, the postulate of maximum dissipation is a physically and mathematically elegant framework. It can be written in the form

$$\sup_{(\boldsymbol{\Sigma}, \boldsymbol{Q}) \in \mathbb{E}_{\boldsymbol{\sigma}}} \mathcal{D} \tag{8}$$

leading to the associative evolution equations and the flow rule

$$\boldsymbol{L}^{\mathrm{p}} = \lambda \, \partial_{\boldsymbol{\Sigma}} \phi \qquad \dot{\boldsymbol{\alpha}} = \lambda \, \partial_{\boldsymbol{Q}} \phi \tag{9}$$

together with the classical Karush-Kuhn-Tucker conditions $\lambda \geq 0$, $\lambda \, \phi \geq 0$. In Eq. (9), λ is the plastic multiplier. According to Eq. (5) and Eq. (9), models showing associative evolution equations can be defined by two independent response functions: the Helmholtz energy and the yield function. Such models are also referred to as *standard dissipative solids*, see Halphen & Nguyen [26].

However, associative rules are not always suitable. This holds in particular for evolution equations characterizing the hardening response. For instance, non-linear hardening of Armstrong-Frederick-type does not fall into the range of standard dissipative solids, see [6]. Consequently, weaker constitutive assumptions are required. A thermodynamically consistent framework for this purpose is that of *generalized standard materials*, cf. [24, 27]. In addition to the yield function ϕ and the Helmholtz energy Ψ, this framework requires an additional response function being the so-called *plastic potential* g. With this potential g, the flow rule and the hardening rules are assumed to be of the type

$$\boldsymbol{L}^{\mathrm{p}} = \lambda \, \partial_{\boldsymbol{\Sigma}} g \qquad \dot{\boldsymbol{\alpha}} = \lambda \, \partial_{\boldsymbol{Q}} g. \tag{10}$$

It can be seen in a straightforward manner that the dissipation resulting from Eq. (10), is always non-negative provided the plastic potential is convex.

2.2 A class of prototype models

According to the previous paragraph, three functions define the mechanical response of a generalized standard material: the Helmholtz energy, the yield function and the plastic potential. In the following, some relatively weak assumptions concerning such functions will be made. They define the class of constitutive models for which variational constitutive updates will be developed in the next sections.

Accounting for isotropic and kinematic hardening, the sets of internal variables $\boldsymbol{\alpha}$ and $\boldsymbol{Q}$ are decomposed accordingly, i.e. $\boldsymbol{\alpha} = (\boldsymbol{\alpha}_\mathrm{k}, \alpha_\mathrm{i})$ and $\boldsymbol{Q} = (\boldsymbol{Q}_\mathrm{k}, Q_\mathrm{i})$. With such notations, the Helmholtz energy (2) is postulated to be of the form

$$\Psi = \Psi^\mathrm{e}(\boldsymbol{F}^\mathrm{e}) + \Psi^\mathrm{p}_\mathrm{k}(\boldsymbol{\alpha}_\mathrm{k}) + \Psi^\mathrm{p}_\mathrm{i}(\alpha_\mathrm{i}), \quad \text{with} \quad \Psi^\mathrm{p}_\mathrm{k}(\boldsymbol{\alpha}_\mathrm{k}) = \frac{1}{2}\, H_\mathrm{k}\, ||\boldsymbol{\alpha}_\mathrm{k}||^2 \tag{11}$$

with H_k being the kinematic hardening modulus. It bears emphasis that enforcing a quadratic function $\Psi^\mathrm{p}_\mathrm{k}$ is not mandatory. However and according to [28], choosing other functions would not modify the respective hardening response essentially.

Based on Eq. (11), the variables energy conjugate to $\boldsymbol{\alpha} = (\boldsymbol{\alpha}_\mathrm{k}, \alpha_\mathrm{i})$ are introduced in standard manner, i.e. $\boldsymbol{Q}_\mathrm{k} = -\partial_{\boldsymbol{\alpha}_\mathrm{k}} \Psi$ and $Q_\mathrm{i} = -\partial_{\alpha_\mathrm{i}} \Psi$. Having defined the stress-like state variables, the yield function can be specified next. Accounting for isotropic as well as for kinematic hardening, a function of the type

$$\phi(\boldsymbol{\Sigma}, \boldsymbol{Q}_\mathrm{k}, Q_\mathrm{i}) = \Sigma^\mathrm{eq}(\boldsymbol{\Sigma} - \boldsymbol{Q}_\mathrm{k}) - Q_\mathrm{i} - Q_0^\mathrm{eq} \tag{12}$$

is a frequently made choice. In Eq. (12), Σ^eq is an equivalent stress measure defining the shape of the yield function ϕ and Q_0^eq is the radius of the initial elastic domain $\mathbb{E}_{\boldsymbol{\sigma}}$. In what follows, it is assumed that Σ^eq is a positively homogeneous function of degree one, i.e.

$$\Sigma^\mathrm{eq}(c\, \boldsymbol{A}) = c\, \Sigma^\mathrm{eq}(\boldsymbol{A}) \quad \forall c \in \mathbb{R}^+. \tag{13}$$

The final assumption is associated with the plastic potential g. Since the focus of the present paper is on variational constitutive updates, variational consistency of the underlying material model has to be guaranteed. It is well known that this is not automatically the case. For this reason, associative evolution equations are postulated here and the only source of non-associativity is related to kinematic hardening. More explicitly, a plastic potential of the form

$$g(\boldsymbol{\Sigma}, \boldsymbol{Q}_\mathrm{k}, Q_\mathrm{i}) = \phi(\boldsymbol{\Sigma}, \boldsymbol{Q}_\mathrm{k}, Q_\mathrm{i}) + \frac{1}{2}\frac{b}{H_\mathrm{k}}\, ||\boldsymbol{Q}_\mathrm{k}||^2 \tag{14}$$

is adopted. It accounts for an Armstrong-Frederick-type saturation of the strain-like internal variable $\boldsymbol{\alpha}_\mathrm{k}$, cf. [6]. The material parameter b in Eq. (14) defines the saturation of the internal variable $\boldsymbol{\alpha}_\mathrm{k}$ (see [6]).

Remark 1 *In Addition to Eqs. (11)-(14), no further assumptions are made. As a result, all functions can be highly anisotropic.*

Remark 2 *Evolution equation $(10)_2$ is based on the material time derivative. It is well known that such a model can lead to unphysical results such as artificial shear oscillations. However, other modified evolution equations for the internal variable $\boldsymbol{\alpha}$ based on objective time derivatives can be easily applied as well. Alternatively, evolution equations based on the so-called* center configuration *could be considered (see [29, 30]). All such modifications are consistently included in the variational constitutive update discussed in the next sections, cf. [6].*

3 Fundamentals of variational constitutive updates

In what follows, the finite strain plasticity model discussed before is rewritten into a variational form, cf. [3, 4, 6, 8]. Physically speaking, the underlying idea of this variational reformulation is the minimization of the stress power. For analogies and differences between this principle and the postulate of maximum dissipation, the interested reader is referred to [5]. Since the foundations of variational constitutive updates can be found in detail in [3, 4, 6, 8], a concise description of those schemes is given here.

Focusing on admissible states, the stress power $\mathcal{E}$ can be written as

$$\mathcal{E} = \boldsymbol{P} : \dot{\boldsymbol{F}} = \dot{\Psi} + \mathcal{D}. \tag{15}$$

According to Eq. (15), $\mathcal{E}$ is decomposed into the rate of the Helmholtz energy Ψ and the dissipation $\mathcal{D}$. Computing the evolution equations (10) for the plastic potential (14) and inserting the resulting equations into the dissipation inequality (6), yields the dissipation

$$\mathcal{D} = \lambda\, Q_0^{\mathrm{eq}} + \lambda\, \frac{b}{H_{\mathrm{k}}}\, ||\boldsymbol{Q}_{\mathrm{k}}||^2. \tag{16}$$

Here, the positive homogeneity of degree one of Σ^{eq} has been used, cf. Eq. (13). Considering these evolution equations once again, the rate of the Helmholtz energy (11) can be written as

$$\dot{\Psi} = \boldsymbol{P} : \dot{\boldsymbol{F}} - \lambda\, \boldsymbol{\Sigma} : \partial_{\boldsymbol{\Xi}}\phi + \boldsymbol{Q}_{\mathrm{k}} : \underbrace{\left(\partial_{\boldsymbol{\Xi}}\phi - \frac{b}{H_{\mathrm{k}}}\, \boldsymbol{Q}_{\mathrm{k}}\right)}_{=\,-\dot{\boldsymbol{\alpha}}_{\mathrm{k}}}\, \lambda - Q_{\mathrm{i}}\, \dot{\alpha}_{\mathrm{i}}, \qquad \boldsymbol{\Xi} := \boldsymbol{\Sigma} - \boldsymbol{Q}_{\mathrm{k}}. \tag{17}$$

Thus, the stress power as predicted by the discussed constitutive framework is given by

$$\mathcal{E}(\dot{\boldsymbol{\varphi}}, \lambda, \boldsymbol{M}) = \dot{\Psi}(\dot{\boldsymbol{\varphi}}, \lambda, \boldsymbol{M}) + \mathcal{D}(\lambda) = \boldsymbol{P} : \dot{\boldsymbol{F}} - \lambda\, \left(\boldsymbol{\Xi} : \partial_{\boldsymbol{\Xi}}\phi - Q_{\mathrm{i}} - Q_0^{\mathrm{eq}}\right). \tag{18}$$

According to Eq. (18), the stress power is regarded as a function of the deformation rate $\dot{\boldsymbol{\varphi}}$, the plastic multiplier λ and a second-order tensor $\boldsymbol{M}$ defining the flow direction, i.e., $\boldsymbol{L}^{\mathrm{p}} = \lambda\, \boldsymbol{M}$ holds. The other state variables such as the relative stresses $\boldsymbol{\Xi}$ or the internal variables Q_{i} are considered as fixed, cf. [3, 4, 6, 8].

The physical relevance of Eq. (18) becomes evident, if its stationarity conditions are computed. More explicitly, stability of $\mathcal{E}$ with respect to the plastic multiplier requires

$$\frac{\partial \mathcal{E}}{\partial \lambda} = -\boldsymbol{\Xi} : \partial_{\boldsymbol{\Xi}}\phi - Q_{\mathrm{i}} - Q_0^{\mathrm{eq}} = -\phi \geq 0. \tag{19}$$

In Eq. (19), the positive homogeneity of degree one of Σ^{eq} resulting in $\partial_{\boldsymbol{\Xi}}\phi : \boldsymbol{\Xi} = \Sigma^{\mathrm{eq}}$ has been used. Thus, stability is equivalent to enforcing physically admissible stresses, i.e. $\phi \leq 0$. Stationarity with respect to the second-order tensor $\boldsymbol{M}$ depends on the parameterization. Formally, the respective condition can be written as

$$\frac{\partial \mathcal{E}}{\partial \boldsymbol{M}} = -\lambda\, \boldsymbol{\Xi} : \partial^2_{\boldsymbol{\Xi}\boldsymbol{M}}\phi = \boldsymbol{0}. \tag{20}$$

In the next sections, it will be shown that Eq. (20) enforces the correct flow rule provided the parameterization is physically sound.

In summary, the resulting variational constitutive update is given by the natural minimization principle

$$(\lambda, \boldsymbol{M}) = \arg \inf_{\lambda, \boldsymbol{M}} \mathcal{E}|_{\dot{\boldsymbol{\varphi}}=\boldsymbol{0}} \tag{21}$$

and the stresses follow subsequently from

$$\boldsymbol{P} = \frac{\partial \left(\arg \inf_{\lambda, \boldsymbol{M}} \mathcal{E}\right)}{\partial \dot{\boldsymbol{F}}} \tag{22}$$

4 On the influence of the flow rule parameterization on variational constitutive updates

In this section, different implementations for variational constitutive updates are critically analyzed. For that purpose, the respective fundamentals are briefly given in Subsection 4.1. Subsequently, two implementations are discussed in detail. The first of those is based on a direct parameterization of the flow rule (see Subsection 4.2), while the second relies on the concept of so-called *pseudo stresses* (see Subsection 4.3).

4.1 Fundamentals

The overriding idea associated with the numerical implementation of variational constitutive updates is very natural: Based on the time-continuous problem (21) (see also Eq. (18)), a discrete approximation

can be obtained by considering a time discretization over the interval $t \in [t_n; t_{n+1}]$. More specifically, introducing the abbreviation $\Delta\lambda := \int_{t_n}^{t_{n+1}} \lambda \, \mathrm{d}t$, the respective discrete optimization problem reads

$$(\Delta\lambda, \boldsymbol{M}) = \arg \inf_{\Delta\lambda, \boldsymbol{M}} I_{\mathrm{inc}} \tag{23}$$

with

$$I_{\mathrm{inc}} = \Psi_{n+1} - \Psi_n + \int_{t_n}^{t_{n+1}} \mathcal{D} \, \mathrm{d}t. \tag{24}$$

Evidently, the underlying equations are highly nonlinear and thus, Eq. (24) cannot be computed analytically in general. For this reason, a time discretization is applied. In this respect, the resulting variational constitutive update is not uniquely defined, but depends on precisely this discretization. However, if a consistent integration is used, consistency of the algorithm is expected. Thus and regardless of the time discretization, the algorithm should converge to the time-continuous problem (21) (see also Eq. (18)) for vanishing time steps ($\Delta t = t_{n+1} - t_n \to 0$). This has to be proved explicitly.

In the present paper, the nonlinear function (24) is computed by employing a standard implicit backward Euler time integration, i.e.

$$I_{\mathrm{inc}} = \Psi_{n+1} - \Psi_n + \Delta\lambda \, Q_0^{\mathrm{eq}} + \Delta\lambda \, \frac{b}{H_{\mathrm{k}}} \, ||\boldsymbol{Q}_{\mathrm{k}}|_{n+1}||^2. \tag{25}$$

Analogously, the evolution laws $\dot{\boldsymbol{\alpha}}_{\mathrm{k}} = \lambda \, \partial_{\boldsymbol{Q}_{\mathrm{k}}} g = -\lambda \, (b \, \boldsymbol{\alpha}_{\mathrm{k}} + \partial_{\boldsymbol{\Xi}} \phi)$ and $\dot{\alpha}_{\mathrm{i}} = \lambda \, \partial_{Q_{\mathrm{i}}} g = -\lambda$ defining the internal variables are also integrated by a standard implicit backward Euler time integration yielding

$$\boldsymbol{\alpha}_{\mathrm{k}}|_{n+1} = \frac{\boldsymbol{\alpha}_{\mathrm{k}}|_n - \Delta\lambda \, \partial_{\boldsymbol{\Xi}} \phi|_{n+1}}{1 + \Delta\lambda \, b}, \qquad \alpha_{\mathrm{i}}|_{n+1} = \alpha_{\mathrm{i}}|_n - \Delta\lambda. \tag{26}$$

Contrariwise, an implicit exponential mapping of the type

$$\boldsymbol{F}_{n+1}^{\mathrm{p}} = \exp\left[\Delta\lambda \, \partial_{\boldsymbol{\Xi}} \phi|_{n+1}\right] \cdot \boldsymbol{F}_n^{\mathrm{p}} \tag{27}$$

is used for the flow rule. Here, $\exp(\bullet)$ is the exponential mapping of second-order tensors, cf. [31]. By inserting Eq. (26) and Eq. (27) into the potential (25), the only unknown variables are the integrated plastic multiplier $\Delta\lambda$ and the flow direction $\boldsymbol{M}$ at time t_{n+1}, i.e., $I_{\mathrm{inc}} = I_{\mathrm{inc}}(\Delta\lambda, \boldsymbol{M})$.

Remark 3 *Similarly to the classical return-mapping scheme, loading is checked by an elastic predictor step. More precisely, stability of the energy I_{inc} requires in this case*

$$\left.\frac{\partial I_{\mathrm{inc}}}{\partial \Delta\lambda}\right|_{\Delta\lambda=0} = -\phi_{n+1}^{\mathrm{trial}} \geq 0. \tag{28}$$

Accordingly, plastic loading is only possible, if $\phi_{n+1}^{\mathrm{trial}} > 0$. For improving the numerical efficiency of the algorithm, the optimization problem (23) is only solved, if $\phi_{n+1}^{\mathrm{trial}} > 0$.

Remark 4 *Since kinematic hardening does not influence the parameterization of the flow rule, it is neglected in what follows.*

4.2 A direct parameterization of the flow rule

The most natural representation of the flow rule is a direct parameterization. Thus, $\boldsymbol{L}^{\mathrm{p}}$ respectively $\Delta\boldsymbol{L}^{\mathrm{p}}$ is the unknown defining the flow direction as well as the plastic multiplier (implicitly). Such a parameterization has already been published in [10] for isotropic models. In this case, $\Delta\boldsymbol{L}^{\mathrm{p}}$ is coaxial to the elastic trial right Cauchy-Green tensor and thus, only the eigenvalues of $\Delta\boldsymbol{L}^{\mathrm{p}}$ are unknown. However, the more general framework discussed in Subsection 2.2 is considered here.

4.2.1 Fundamentals

Choosing $\Delta\boldsymbol{L}^{\mathrm{p}}$ as the unknown within the variational constitutive update, the exponential mapping (27) reads

$$\boldsymbol{F}_{n+1}^{\mathrm{e}} = \boldsymbol{F}^{\mathrm{e\,trial}} \cdot \exp\left[-\Delta\boldsymbol{L}_{n+1}^{\mathrm{p}}\right], \quad \text{with} \quad \boldsymbol{F}^{\mathrm{e\,trial}} := \boldsymbol{F}_{n+1} \cdot \boldsymbol{F}_n^{\mathrm{p}\,-1}. \tag{29}$$

Using this parameterization, the integrated plastic multiplier is computed as

$$\Delta\lambda = \frac{||\Delta \boldsymbol{L}^{\mathrm{p}}_{n+1}||}{||\partial_{\boldsymbol{\Sigma}}\phi|_{n+1}||}. \tag{30}$$

Unfortunately, this function cannot be solved in closed form in general. For instance, if ϕ is anisotropic, $||\partial_{\boldsymbol{\Sigma}}\phi|_{n+1}||$ is not constant, but it depends on the final stress state. However, even for fully isotropic models (yield function and hardening) and equivalent stresses Σ^{eq} being positively homogeneous of degree one, $||\partial_{\boldsymbol{\Sigma}}\phi|_{n+1}||$ is not constant in general. One such example is given by the equivalent stress $\Sigma^{\mathrm{eq}} = \sqrt{\Sigma_1\,\Sigma_2}$ with Σ_i denoting the eigenvalues of the Mandel stress tensor $\boldsymbol{\Sigma}$.

Although the aforementioned parameterization can be modified for yield functions not fulfilling the constraint $||\partial_{\boldsymbol{\Sigma}}\phi|_{n+1}|| = \text{const}$ (see Remark 5), such modifications are not discussed in detail here. For this reason, the assumption

$$c := ||\partial_{\boldsymbol{\Sigma}}\phi|_{n+1}|| = \text{const} \tag{31}$$

is made. It is, for instance, fulfilled for the family of Drucker-Prager-type yield functions

$$\phi = \gamma\ \mathrm{tr}\,\boldsymbol{\Sigma} + \theta\ ||\,\mathrm{dev}\,\boldsymbol{\Sigma}|| - Q_{\mathrm{i}} - Q_0^{\mathrm{eq}} \quad \text{with} \quad \mathrm{tr}\boldsymbol{\Sigma} = \boldsymbol{1} : \boldsymbol{\Sigma}, \quad \mathrm{dev}\,\boldsymbol{\Sigma} = \boldsymbol{\Sigma} - \frac{1}{3}\,\mathrm{tr}\boldsymbol{\Sigma}\,\boldsymbol{1} \tag{32}$$

containing, among others, the von Mises ($\gamma = 0$, $\theta = 1$) as well as a purely volumetric yield function ($\gamma = 1$, $\theta = 0$). With this choice, the integrated stress power (25) without kinematic hardening reads

$$I_{\mathrm{inc}} = \Psi_{n+1}(\boldsymbol{F}_{n+1}, \Delta \boldsymbol{L}^{\mathrm{p}}_{n+1}) - \Psi_n + \frac{1}{c}\ ||\Delta \boldsymbol{L}^{\mathrm{p}}_{n+1}||\ Q_0^{\mathrm{eq}}. \tag{33}$$

Based on Eq. (33), the unknown incremental plastic flow $\Delta \boldsymbol{L}^{\mathrm{p}}_{n+1}$ can be computed from the minimization principle

$$\Delta \boldsymbol{L}^{\mathrm{p}}_{n+1} = \arg \inf_{\Delta \boldsymbol{L}^{\mathrm{p}}_{n+1}} I_{\mathrm{inc}}|_{\boldsymbol{F}_{n+1}=\mathrm{const}}\,. \tag{34}$$

However, a direct unconstrained minimization of I_{inc} would not lead to physically sound results, since the constraints implied by the flow rule have not been considered within the parameterization yet. For enforcing such constraints, a simple projection technique is employed within the present subsection. Introducing the arbitrary tensor $\tilde{\boldsymbol{K}} \in \mathbb{R}^9$, this technique can be formally written as

$$\Delta \boldsymbol{L}^{\mathrm{p}}_{n+1} = \mathbb{P} : \tilde{\boldsymbol{K}} \tag{35}$$

Here, $\mathbb{P}$ represents the respective projection operator. According to Eq. (35), the tensor $\tilde{\boldsymbol{K}}$ can be interpreted as the incremental plastic flow without considering the constraints induced by the flow rule. For instance, $\mathbb{P}$ is the deviatoric projection $\mathbb{P} = \mathbb{I} - \frac{1}{3}\boldsymbol{1} \otimes \boldsymbol{1}$ in case of a von Mises yield function. Clearly, symmetry of $\Delta \boldsymbol{L}^{\mathrm{p}}$ could be guaranteed by using a similar technique. However, this is enforced directly within the present implementation by setting explicitly $[\Delta \boldsymbol{L}^{\mathrm{p}}]_{21} = [\Delta \boldsymbol{L}^{\mathrm{p}}]_{12}$.

Employing the aforementioned projection technique, the necessary condition associated with Eq. (34) is computed as

$$\begin{aligned} \frac{\partial I_{\mathrm{inc}}}{\partial \Delta \boldsymbol{L}^{\mathrm{p}}_{n+1}} : \frac{\partial \Delta \boldsymbol{L}^{\mathrm{p}}_{n+1}}{\partial \tilde{\boldsymbol{K}}} = \Big[& \underbrace{-\boldsymbol{\Sigma}^{\star}_{n+1} : \mathrm{Dexp}\left[-\Delta \boldsymbol{L}^{\mathrm{p}}_{n+1}\right]}_{= \partial\Psi/\partial \Delta \boldsymbol{L}^{\mathrm{p}}_{n+1}} \\ & + \frac{1}{c}\ \frac{\Delta \boldsymbol{L}^{\mathrm{p}}_{n+1}}{||\Delta \boldsymbol{L}^{\mathrm{p}}_{n+1}||}\ (Q_{\mathrm{i}} + Q_0^{\mathrm{eq}}) \Big] : \mathbb{P} = \boldsymbol{0} \end{aligned} \tag{36}$$

with

$$\boldsymbol{\Sigma}^{\star}_{n+1} := (\boldsymbol{F}^{\mathrm{e\,trial}})^T \cdot \boldsymbol{P}^{\mathrm{e}}_{n+1}. \tag{37}$$

In Eq. (36), Dexp($\bullet$) represents the first derivative of the exponential mapping with respect to ($\bullet$). Eq. (36) can be efficiently solved by means of Newton's method. This will be discussed in the next subsection.

For showing consistency of the algorithm, stationarity condition (36) is analyzed for $\Delta t \to 0$. In this case, $\mathrm{Dexp}\left[-\Delta \boldsymbol{L}^{\mathrm{p}}_{n+1}\right] \to \mathbb{I}$ and $\boldsymbol{\Sigma}^{\star}_{n+1} \to \boldsymbol{\Sigma}_{n+1}$ leading to

$$\left.\frac{\partial I_{\mathrm{inc}}}{\partial \tilde{\boldsymbol{K}}_{n+1}}\right|_{\Delta t\to 0} = \left[-\boldsymbol{\Sigma}_{n+1} + \frac{1}{c}\,\frac{\Delta \boldsymbol{L}^{\mathrm{p}}_{n+1}}{||\Delta \boldsymbol{L}^{\mathrm{p}}_{n+1}||}\;(Q_{\mathrm{i}} + Q_0^{\mathrm{eq}})\right] : \mathbb{P} = \boldsymbol{0}. \tag{38}$$

This is equivalent to the flow rule

$$\Delta \boldsymbol{L}^{\mathrm{p}}_{n+1} : \mathbb{P} = \frac{||\Delta \boldsymbol{L}^{\mathrm{p}}_{n+1}||\; c}{Q_{\mathrm{i}} + Q_0^{\mathrm{eq}}}\;\boldsymbol{\Sigma}_{n+1} : \mathbb{P}. \tag{39}$$

Thus, if $\mathbb{P}$ is a projection in the sense of linear algebra ($\mathbb{P} : \mathbb{P} = \mathbb{P}$), Eq. (39) results in

$$\Delta \boldsymbol{L}^{\mathrm{p}}_{n+1} = \frac{||\Delta \boldsymbol{L}^{\mathrm{p}}_{n+1}||\; c}{\Sigma^{\mathrm{eq}}}\;\boldsymbol{\Sigma}_{n+1} : \mathbb{P} \tag{40}$$

where the identity $\Sigma^{\mathrm{eq}} = Q_0^{\mathrm{eq}} + Q_{\mathrm{i}}$ holding for plastic loading has been used. Consistency of Eq. (40) can be verified in a straightforward manner. For instance, in case of von Mises plasticity ($\gamma = 0$, $\theta = 1$, $\Sigma^{\mathrm{eq}} = ||\operatorname{dev}\boldsymbol{\Sigma}||$, $\mathbb{P} = \mathbb{I} - \frac{1}{3}\boldsymbol{1}\otimes\boldsymbol{1}$), Eq. (40) yields

$$\Delta \boldsymbol{L}^{\mathrm{p}}_{n+1} = ||\Delta \boldsymbol{L}^{\mathrm{p}}_{n+1}||\;\frac{\operatorname{dev}\boldsymbol{\Sigma}_{n+1}}{||\operatorname{dev}\boldsymbol{\Sigma}_{n+1}||}, \tag{41}$$

while a shear independent yield function ($\gamma = 1$, $\theta = 0$, $\Sigma^{\mathrm{eq}} = \boldsymbol{1} : \operatorname{dev}\boldsymbol{\Sigma}$, $\mathbb{P} = \frac{1}{3}\boldsymbol{1}\otimes\boldsymbol{1}$) gives

$$\Delta \boldsymbol{L}^{\mathrm{p}}_{n+1} = ||\Delta \boldsymbol{L}^{\mathrm{p}}_{n+1}||\;\boldsymbol{1}. \tag{42}$$

Evidently, both equations comply with the underlying yield functions and associative flow rules. As a result, the variational constitutive update naturally enforces the correct flow rule.

Finally, it will be shown that the advocated variational framework also includes the yield function, i.e., it avoids inadmissible states. For verifying this, the condition of energy stability is rewritten as

$$\left.\frac{\partial I_{\mathrm{inc}}}{\partial \tilde{\boldsymbol{K}}_{n+1}}\right|_{\Delta t\to 0} : \boldsymbol{A} \geq 0 \qquad \forall \boldsymbol{A}. \tag{43}$$

Choosing $\boldsymbol{A}$ as the incremental plastic flow, i.e. $\boldsymbol{A} = \Delta \boldsymbol{L}^{\mathrm{p}}_{n+1}$, Eq. (43) implies

$$\left.\frac{\partial I_{\mathrm{inc}}}{\partial \tilde{\boldsymbol{K}}_{n+1}}\right|_{\Delta t\to 0} : \Delta \boldsymbol{L}^{\mathrm{p}}_{n+1} = -\left[c\,\frac{||\boldsymbol{\Sigma} : \mathbb{P}||^2}{\Sigma^{\mathrm{eq}}} - (Q_0^{\mathrm{eq}} + Q_{\mathrm{i}})\right]\;||\boldsymbol{L}^{\mathrm{p}}_{n+1}|| \geq 0 \tag{44}$$

$$\Rightarrow \left[c\,\frac{||\boldsymbol{\Sigma} : \mathbb{P}||^2}{\Sigma^{\mathrm{eq}}} - (Q_0^{\mathrm{eq}} + Q_{\mathrm{i}})\right] \leq 0. \tag{45}$$

Again, a straightforward computation shows that Ineq. (45) is equivalent to $\phi \leq 0$. In case of von Mises plasticity ($\gamma = 0$, $\theta = 1$, $\Sigma^{\mathrm{eq}} = ||\operatorname{dev}\boldsymbol{\Sigma}||$) or a shear independent yield function ($\gamma = 1$, $\theta = 0$, $\Sigma^{\mathrm{eq}} = \boldsymbol{1} : \operatorname{dev}\boldsymbol{\Sigma}$, $\mathbb{P} = \frac{1}{3}\boldsymbol{1}\otimes\boldsymbol{1}$) this can be directly seen. In summary, the variational reformulation (34) combined with the projection method is thus consistent.

Remark 5 *One way of modifying the proposed algorithm for isotropic yield functions not fulfilling the constraint $||\partial_{\boldsymbol{\Sigma}}\phi|| = \mathrm{const}$ is the application of an explicit/implicit integration scheme of the type*

$$\Delta\lambda = \frac{||\boldsymbol{L}^{\mathrm{p}}_{n+1}||}{||\partial_{\boldsymbol{\Sigma}}\phi|_n||}. \tag{46}$$

However, such purely numerically motivated modifications will not be discussed in detail here.

4.2.2 Numerical implementation

Eq. (36) is efficiently solved by means of Newton's method. For that purpose, the residual (36) has to be linearized resulting in the set of linear equations

$$\frac{\partial I_{\mathrm{inc}}}{\partial \tilde{\boldsymbol{K}}} + \frac{\partial^2 I_{\mathrm{inc}}}{\partial \tilde{\boldsymbol{K}}^2} : \Delta\tilde{\boldsymbol{K}} = \boldsymbol{0} \quad \Rightarrow \quad \Delta\tilde{\boldsymbol{K}}. \tag{47}$$

By combining the chain rule

$$\frac{\partial^2 I_{\text{inc}}}{\partial \tilde{\boldsymbol{K}}^2} = \mathbb{P}^T : \frac{\partial^2 I_{\text{inc}}}{\partial (\boldsymbol{L}^{\text{p}}_{n+1})^2} : \mathbb{P}, \qquad [\mathbb{P}^T]_{ijkl} = [\mathbb{P}]_{klij} \tag{48}$$

with

$$\begin{aligned}\frac{\partial^2 I_{\text{inc}}}{\partial (\boldsymbol{L}^{\text{p}}_{n+1})^2} = \left.\frac{\partial \boldsymbol{\Sigma}^\star}{\partial \boldsymbol{F}^{\text{e}}}\right|_{n+1} \overset{(1)}{\cdot} \text{Dexp}\left[-\boldsymbol{L}^{\text{p}}_{n+1}\right] \overset{(3)}{\cdot} \text{Dexp}\left[-\boldsymbol{L}^{\text{p}}_{n+1}\right] - \boldsymbol{\Sigma}^\star_{n+1} : \text{D}^2\text{exp}\left[-\boldsymbol{L}^{\text{p}}_{n+1}\right] \\ + \frac{1}{c} \left.\frac{\partial^2 ||\boldsymbol{L}^{\text{p}}_{n+1}||}{\partial (\boldsymbol{L}^{\text{p}}_{n+1})^2}\right|_{n+1} (Q_{\text{i}} + Q_0^{\text{eq}})\end{aligned} \tag{49}$$

the Hessian matrix $\partial^2 I_{\text{inc}}/\partial \tilde{\boldsymbol{K}}^2$ can be computed. Here, the terms

$$\left.\frac{\partial \boldsymbol{\Sigma}^\star}{\partial \boldsymbol{F}^{\text{e}}}\right|_{n+1} = (\boldsymbol{F}^{\text{e trial}})^T \cdot \left.\frac{\partial \boldsymbol{P}^{\text{e}}}{\partial \boldsymbol{F}^{\text{e}}}\right|_{n+1} \overset{(3)}{\cdot} \boldsymbol{F}^{\text{e trial}} \tag{50}$$

and

$$\frac{\partial^2 ||\boldsymbol{L}^{\text{p}}_{n+1}||}{\partial (\boldsymbol{L}^{\text{p}}_{n+1})^2} = \frac{1}{||\boldsymbol{L}^{\text{p}}_{n+1}||} \left[\boldsymbol{1} \,\overline{\otimes}\, \boldsymbol{1} - \frac{\partial ||\boldsymbol{L}^{\text{p}}_{n+1}||}{\partial \boldsymbol{L}^{\text{p}}_{n+1}} \otimes \frac{\partial ||\boldsymbol{L}^{\text{p}}_{n+1}||}{\partial \boldsymbol{L}^{\text{p}}_{n+1}}\right] \tag{51}$$

have been introduced. Furthermore $(\boldsymbol{1} \,\overline{\otimes}\, \boldsymbol{1})_{ijkl} = \delta_{ik}\delta_{jl}$ denotes the fourth-order identity tensor, $\text{D}^2\text{exp}(\bullet)$ is the second derivative of the exponential mapping with respect to its argument $(\bullet)$ and the index i in the expression $\overset{(i)}{\cdot}$ indicates the first component of the tensor on the right hand side over which the summation has to be performed, i.e. $[\boldsymbol{a} \overset{(2)}{\cdot} \mathbb{C}]_{jkl} = a_i\, \mathbb{C}_{jikl}$ and $[\boldsymbol{A} \overset{(2)}{\cdot} \mathbb{C}]_{il} = A_{jk}\, \mathbb{C}_{ijkl}$. It bears emphasis that standard projections $\mathbb{P}$ show major symmetry and thus, $\mathbb{P}^T = \mathbb{P}$.

For obtaining an asymptotically quadratic convergence also on the structural level, the consistent tangent moduli are required. They follow from the linearization

$$\text{d}\boldsymbol{P} = \text{d}\left(\frac{\partial I_{\text{inc}}}{\partial \boldsymbol{F}}\right) = \underbrace{\left[\frac{\partial^2 I_{\text{inc}}}{\partial \boldsymbol{F}^2} + \frac{\partial^2 I_{\text{inc}}}{\partial \boldsymbol{F} \partial \tilde{\boldsymbol{K}}} : \frac{\text{d}\tilde{\boldsymbol{K}}}{\text{d}\boldsymbol{F}}\right]}_{= \text{d}\boldsymbol{P}/\text{d}\boldsymbol{F}} : \text{d}\boldsymbol{F}. \tag{52}$$

The derivative $\text{d}\tilde{\boldsymbol{K}}/\text{d}\boldsymbol{F}$ in Eq. (52) is computed by linearizing the residual (36) at a converged stage. More explicitly, considering $\partial I_{\text{inc}}/\partial \tilde{\boldsymbol{K}} = \boldsymbol{0}$ yields

$$\frac{\text{d}\tilde{\boldsymbol{K}}}{\text{d}\boldsymbol{F}} = -\left[\frac{\partial^2 I_{\text{inc}}}{\partial \tilde{\boldsymbol{K}}^2}\right]^{-1} : \frac{\partial^2 I_{\text{inc}}}{\partial \tilde{\boldsymbol{K}} \partial \boldsymbol{F}}. \tag{53}$$

Here, the mixed derivative is given by

$$\frac{\partial^2 I_{\text{inc}}}{\partial \tilde{\boldsymbol{K}} \partial \boldsymbol{F}} = -\left[\frac{\partial \boldsymbol{\Sigma}^\star}{\partial \boldsymbol{F}^{\text{e}}} : \frac{\partial \boldsymbol{F}^{\text{e}}}{\partial \boldsymbol{F}}\right] \overset{(1)}{\cdot} \text{Dexp}\left[-\Delta \boldsymbol{L}^{\text{p}}_{n+1}\right] : \mathbb{P}. \tag{54}$$

By inserting Eq. (54) into Eq. (53) and combing the result with Eq. (52), the consistent tangent moduli are finally obtained as

$$\frac{\text{d}\boldsymbol{P}_{n+1}}{\text{d}\boldsymbol{F}_{n+1}} = \frac{\partial^2 I_{\text{inc}}}{\partial \boldsymbol{F}^2_{n+1}} - \frac{\partial^2 I_{\text{inc}}}{\partial \boldsymbol{F}_{n+1} \partial \tilde{\boldsymbol{K}}} : \left[\frac{\partial^2 I_{\text{inc}}}{\partial \tilde{\boldsymbol{K}}^2}\right]^{-1} : \frac{\partial^2 I_{\text{inc}}}{\partial \tilde{\boldsymbol{K}} \partial \boldsymbol{F}_{n+1}}. \tag{55}$$

As can be seen from Eq. (55), the tangent matrix automatically preserves the symmetric structure of the underlying constitutive model. This is a direct consequence of the variationally consistency of the approach.

4.2.3 Concluding remarks

By rewriting the gradient (36) into the residual form

$$\boldsymbol{R}(\tilde{\boldsymbol{K}}) := \frac{\partial I_{\text{inc}}}{\partial \tilde{\boldsymbol{K}}}, \tag{56}$$

the proposed algorithm can be compared to the classical return-mapping scheme, cf. [1, 2]. By doing so, two things can be observed. First, both algorithms are based on the same time integration scheme and the underlying residuals show a similar structure. However, while the standard residual of the return mapping scheme is ten-dimensional ($\dim \boldsymbol{F}^{\mathrm{p}} + \dim \lambda = 10$), the variational constitutive update is formulated in a space with reduced complexity. The dimension of that space is defined by the rank of the projection operator $\mathbb{P}$. In this connection, the upper bound is nine ($\dim \tilde{\boldsymbol{K}}$). However, for many practically relevant constitutive models the rank of $\mathbb{P}$ is significantly less that nine. For instance, in case of a von Mises yield function ($\mathrm{tr}\, \boldsymbol{L}^{\mathrm{p}} = 0$) and elastic isotropy ($\boldsymbol{\Sigma} = \boldsymbol{\Sigma}^T$), the residual (56) is five-dimensional. By summarizing the aforementioned points, it is expected that the proposed variational constitutive update is slightly numerically more efficient than the classical return-mapping scheme and that it shows a similar numerical stability. This could be verified by numerical experiments which will be shown in Section 6.

Besides the positive features of the analyzed variational constitutive update, the resulting algorithm has also some shortcomings. More precisely, it can only be applied, if the respective yield function is fully isotropic. Furthermore, the norm of the flow direction has to be constant, cf. Remark 5. This narrows the range of application considerably.

4.3 A parameterization of the flow rule direction by using pseudo stresses

A parameterization not showing such shortcomings was proposed in the series of paper [6, 10, 18, 19]. It is based on the concept of so-called *pseudo stresses*. In what follows, the fundamentals of this parameterization, together with a complete description of a numerical implementation by means of Newton's method, will be given. Finally, the resulting algorithm is critically analyzed.

4.3.1 Fundamentals

In contrast to the previously discussed direct parameterization (29) of $\Delta \boldsymbol{L}^{\mathrm{p}}_{n+1}$, the flow direction is defined here by employing the concept of pseudo stresses. Such stresses denoted as $\tilde{\boldsymbol{\Sigma}}$ are not identical to their physical counterparts $\boldsymbol{\Sigma}$. Based on $\tilde{\boldsymbol{\Sigma}}$, the flow rule is parameterized by

$$\boldsymbol{L}^{\mathrm{p}}(\lambda, \tilde{\boldsymbol{\Sigma}}) = \lambda\, \partial_{\boldsymbol{\Sigma}} \phi|_{\boldsymbol{\Sigma}=\tilde{\boldsymbol{\Sigma}}}. \tag{57}$$

Accordingly, the flow rule is evaluated for the pseudo stresses. By doing so, all constraints induced by the yield function are naturally included. For instance, in cases of von Mises plasticity,

$$\mathbf{1} : \partial_{\boldsymbol{\Sigma}} \phi|_{\boldsymbol{\Sigma}=\tilde{\boldsymbol{\Sigma}}} = 0 \qquad \forall \tilde{\boldsymbol{\Sigma}} \tag{58}$$

is automatically fulfilled and thus, the flow is purely deviatoric. A further advantage of this concept is the decomposition of the plastic strain rate into a direction and an amplitude. Hence, the plastic multiplier is explicitly used within this framework and does not need to be computed implicitly, see Eq. (30).

Employing the aforementioned parameterization, the plastic part of the deformation gradient at time t_{n+1} can be computed as

$$\boldsymbol{F}^{\mathrm{e}}_{n+1} = \boldsymbol{F}^{\mathrm{e\,trial}} \cdot \exp\left[-\Delta\lambda\, \partial_{\boldsymbol{\Sigma}} \phi|_{\boldsymbol{\Sigma}=\tilde{\boldsymbol{\Sigma}}}\right], \quad \text{with} \quad \boldsymbol{F}^{\mathrm{e\,trial}} := \boldsymbol{F}_{n+1} \cdot \boldsymbol{F}^{\mathrm{p}\,-1}_{n} \tag{59}$$

where $\tilde{\boldsymbol{\Sigma}}$ are the pseudo stresses at time t_{n+1}, i.e., an implicit integration scheme is considered. As a result, the variational constitutive update reads now

$$\begin{aligned} (\Delta\lambda, \tilde{\boldsymbol{\Sigma}}) = \arg \inf_{\Delta\lambda, \tilde{\boldsymbol{\Sigma}}} I_{\mathrm{inc}}|_{\boldsymbol{F}_{n+1}=\mathrm{const}}, \qquad \boldsymbol{P} = \partial_{\boldsymbol{F}_{n+1}} \inf_{\Delta\lambda, \tilde{\boldsymbol{\Sigma}}} I_{\mathrm{inc}} \\ I_{\mathrm{inc}} = \Psi_{n+1}(\boldsymbol{F}_{n+1}, \Delta\lambda, \tilde{\boldsymbol{\Sigma}}) - \Psi_n + \Delta\lambda\, Q^{\mathrm{eq}}_0. \end{aligned} \tag{60}$$

Again, kinematic hardening has been neglected, since it does not modify the resulting algorithm essentially, cf. [6]. It bears emphasis that a positive plastic multiplier has to be enforced in Eq. (60). This can be implemented either by inserting $\Delta\lambda = a^2$ or by replacing $\Delta\lambda$ by its absolute value. Within the numerical simulations it turned out that the latter concept was numerically more stable.

For solving minimization problem (60), Newton's method is employed. The respective residual of that scheme reads

$$\boldsymbol{R}(\Delta\lambda, \tilde{\boldsymbol{\Sigma}}) = [\boldsymbol{R}_{\Delta\lambda}(\Delta\lambda, \tilde{\boldsymbol{\Sigma}}); \boldsymbol{R}_{\tilde{\boldsymbol{\Sigma}}}(\Delta\lambda, \tilde{\boldsymbol{\Sigma}})] \tag{61}$$

with

$$\boldsymbol{R}_{\Delta\lambda}(\Delta\lambda,\tilde{\boldsymbol{\Sigma}}) = \frac{\partial I_{\mathrm{inc}}}{\partial \Delta\lambda} = \boldsymbol{\Sigma}^{\star}_{n+1} : \boldsymbol{T}_1 + Q_{\mathrm{i}} + Q_0^{\mathrm{eq}}, \tag{62}$$

$$\boldsymbol{R}_{\tilde{\boldsymbol{\Sigma}}}(\Delta\lambda,\tilde{\boldsymbol{\Sigma}}) = \frac{\partial I_{\mathrm{inc}}}{\partial \tilde{\boldsymbol{\Sigma}}} = \boldsymbol{\Sigma}^{\star}_{n+1} : \mathbb{T}_2. \tag{63}$$

Here and henceforth, the abbreviations $\Delta\boldsymbol{L}^{\mathrm{p}}_{n+1} = \Delta\lambda\, \partial_{\boldsymbol{\Sigma}}\phi|_{\boldsymbol{\Sigma}=\tilde{\boldsymbol{\Sigma}}}$, Eq. (37) and

$$\boldsymbol{T}_1 := - \quad \mathrm{Dexp}\left[-\Delta\boldsymbol{L}^{\mathrm{p}}_{n+1}\right] : \partial_{\boldsymbol{\Sigma}}\phi|_{\boldsymbol{\Sigma}=\tilde{\boldsymbol{\Sigma}}} \tag{64}$$

$$\mathbb{T}_2 := -\Delta\lambda_{n+1}\ \mathrm{Dexp}\left[-\Delta\boldsymbol{L}^{\mathrm{p}}_{n+1}\right] : \partial^2_{\boldsymbol{\Sigma}}\phi\big|_{\boldsymbol{\Sigma}=\tilde{\boldsymbol{\Sigma}}} \tag{65}$$

are used. Starting from Eq. (62) and Eq. (63), consistency of the algorithm can be easily verified. More specifically, evaluating such equations for $\Delta t \to 0$ gives $\boldsymbol{T}_1 = -\ \partial_{\boldsymbol{\Sigma}}\phi|_{\boldsymbol{\Sigma}=\tilde{\boldsymbol{\Sigma}}}$ and $\mathbb{T}_2 = -\Delta\lambda_{n+1}\ \partial^2_{\boldsymbol{\Sigma}}\phi\big|_{\boldsymbol{\Sigma}=\tilde{\boldsymbol{\Sigma}}}$. Combining this with $\boldsymbol{\Sigma}^{\star}_{n+1} = \boldsymbol{\Sigma}_{n+1}$ $(\Delta t \to 0)$ yields

$$\left.\frac{\partial I_{\mathrm{inc}}}{\partial \Delta\lambda}\right|_{\Delta t\to 0} = - \quad \boldsymbol{\Sigma}_{n+1} : \partial_{\boldsymbol{\Sigma}}\phi|_{\boldsymbol{\Sigma}=\tilde{\boldsymbol{\Sigma}}} + Q_{\mathrm{i}} + Q_0^{\mathrm{eq}} = -\phi \tag{66}$$

$$\left.\frac{\partial I_{\mathrm{inc}}}{\partial \tilde{\boldsymbol{\Sigma}}}\right|_{\Delta t\to 0} = -\Delta\lambda_{n+1}\, \boldsymbol{\Sigma}_{n+1} : \partial^2_{\boldsymbol{\Sigma}}\phi\big|_{\boldsymbol{\Sigma}=\tilde{\boldsymbol{\Sigma}}} \tag{67}$$

According to Eq. (66), stability of I_{inc} with respect to the plastic multiplier leads to $\phi \leq 0$ and hence, it naturally avoids inadmissible stress states. Furthermore, stationarity condition $\partial I_{\mathrm{inc}}/\partial\tilde{\boldsymbol{\Sigma}} = \boldsymbol{0}$ is a compatibility condition between the stresses $\boldsymbol{\Sigma}$ and their pseudo counterparts $\tilde{\boldsymbol{\Sigma}}$. The physical interpretation of this equation becomes more obvious, if the positive homogeneity of degree one of the equivalent stress Σ^{eq} is accounted for. With this condition,

$$\Sigma^{\mathrm{eq}} = \partial_{\boldsymbol{\Sigma}}\Sigma^{\mathrm{eq}} : \boldsymbol{\Sigma} \quad \Rightarrow \quad \boldsymbol{\Sigma} : \frac{\partial^2\phi}{\partial\boldsymbol{\Sigma}^2} = \boldsymbol{0} \tag{68}$$

can be derived. Thus, comparing Eq. $(68)_2$ to Eq. (67) shows that the stationarity condition $\partial I_{\mathrm{inc}}/\partial\tilde{\boldsymbol{\Sigma}} = \boldsymbol{0}$ enforces the correct flow rule. As a result, the variational constitutive update based on pseudo stresses is consistent as well.

4.3.2 Numerical implementation

The second derivatives of I_{inc} necessary for Newton's method result eventually in

$$\frac{\partial^2 I_{\mathrm{inc}}}{\partial\Delta\lambda^2} = \frac{\partial\boldsymbol{\Sigma}^{\star}}{\partial\boldsymbol{F}^{\mathrm{e}}} \overset{(1)}{\vdots} \boldsymbol{T}_1 \overset{(3)}{\vdots} \boldsymbol{T}_1 + \boldsymbol{\Sigma}^{\star} : \boldsymbol{T}_3 + \frac{\partial Q_{\mathrm{i}}}{\partial\Delta\lambda}, \tag{69}$$

$$\frac{\partial^2 I_{\mathrm{inc}}}{\partial\Delta\lambda\,\partial\tilde{\boldsymbol{\Sigma}}} = \frac{\partial\boldsymbol{\Sigma}^{\star}}{\partial\boldsymbol{F}^{\mathrm{e}}} \overset{(1)}{\vdots} \boldsymbol{T}_1 \overset{(3)}{\vdots} \mathbb{T}_2 + \boldsymbol{\Sigma}^{\star} : \mathbb{T}_4 + \boldsymbol{\Sigma}^{\star} : \mathbb{T}_2, \tag{70}$$

$$\frac{\partial^2 I_{\mathrm{inc}}}{\partial\tilde{\boldsymbol{\Sigma}}^2} = \frac{\partial\boldsymbol{\Sigma}^{\star}}{\partial\boldsymbol{F}^{\mathrm{e}}} \overset{(1)}{\vdots} \mathbb{T}_2 \overset{(3)}{\vdots} \mathbb{T}_2 + \boldsymbol{\Sigma}^{\star} : \mathcal{T}_5 + \boldsymbol{\Sigma}^{\star} : \mathcal{T}_6. \tag{71}$$

where the notations

$$\boldsymbol{T}_3 := \quad \mathrm{D}^2\mathrm{exp}\left[-\Delta\boldsymbol{L}^{\mathrm{p}}_{n+1}\right] \overset{(3)}{\vdots} \partial_{\boldsymbol{\Sigma}}\phi|_{\boldsymbol{\Sigma}=\tilde{\boldsymbol{\Sigma}}} \overset{(5)}{\vdots} \partial_{\boldsymbol{\Sigma}}\phi|_{\boldsymbol{\Sigma}=\tilde{\boldsymbol{\Sigma}}}\,, \tag{72}$$

$$\mathbb{T}_4 := \quad \Delta\lambda_{n+1}\ \mathrm{D}^2\mathrm{exp}\left[-\Delta\boldsymbol{L}^{\mathrm{p}}_{n+1}\right] \overset{(3)}{\vdots} \partial^2_{\boldsymbol{\Sigma}}\phi\big|_{\boldsymbol{\Sigma}=\tilde{\boldsymbol{\Sigma}}} \overset{(5)}{\vdots} \partial_{\boldsymbol{\Sigma}}\phi|_{\boldsymbol{\Sigma}=\tilde{\boldsymbol{\Sigma}}}\,, \tag{73}$$

$$\mathcal{T}_5 := \quad \Delta\lambda^2_{n+1}\ \mathrm{D}^2\mathrm{exp}\left[-\Delta\boldsymbol{L}^{\mathrm{p}}_{n+1}\right] \overset{(3)}{\vdots} \partial^2_{\boldsymbol{\Sigma}}\phi\big|_{\boldsymbol{\Sigma}=\tilde{\boldsymbol{\Sigma}}} \overset{(5)}{\vdots} \partial^2_{\boldsymbol{\Sigma}}\phi\big|_{\boldsymbol{\Sigma}=\tilde{\boldsymbol{\Sigma}}}\,, \tag{74}$$

$$\mathcal{T}_6 := -\Delta\lambda_{n+1}\quad \mathrm{Dexp}\left[-\Delta\boldsymbol{L}^{\mathrm{p}}_{n+1}\right] \ : \ \partial^3_{\boldsymbol{\Sigma}}\phi\big|_{\boldsymbol{\Sigma}=\tilde{\boldsymbol{\Sigma}}} \tag{75}$$

have been introduced. Since, I_{inc} is sufficiently smooth (in case of a plastic load step), $\partial^2_{\Delta\lambda\,\tilde{\boldsymbol{\Sigma}}} I_{\mathrm{inc}} = \partial^2_{\tilde{\boldsymbol{\Sigma}}\,\Delta\lambda} I_{\mathrm{inc}}$. The additional derivatives with respect to the deformation gradient required for the consistent tangent moduli are given by

$$\frac{\partial^2 I_{\mathrm{inc}}}{\partial\Delta\lambda\,\partial\boldsymbol{F}} = \left[\frac{\partial\boldsymbol{\Sigma}^{\star}}{\partial\boldsymbol{F}^{\mathrm{e}}} : \frac{\partial\boldsymbol{F}^{\mathrm{e}}}{\partial\boldsymbol{F}}\right] \overset{(1)}{\vdots} \boldsymbol{T}_1, \tag{76}$$

$$\frac{\partial^2 I_{\mathrm{inc}}}{\partial\tilde{\boldsymbol{\Sigma}}\,\partial\boldsymbol{F}} = \left[\frac{\partial\boldsymbol{\Sigma}^{\star}}{\partial\boldsymbol{F}^{\mathrm{e}}} : \frac{\partial\boldsymbol{F}^{\mathrm{e}}}{\partial\boldsymbol{F}}\right] \overset{(1)}{\vdots} \mathbb{T}_2. \tag{77}$$

For the sake of conciseness, no further explicit details about the Hessian matrix as well as the tangent moduli will be given here. They will be discussed in detail in the next section where an extended version of the variational constitutive update based on pseudo stresses will be elaborated.

4.3.3 Concluding remarks

The most important advantage of the algorithm described in the present subsection is its range of application. Except for the positive homogeneity of degree one of Σ^{eq} no further assumption is required. Consequently, arbitrary anisotropic yield functions are consistently included within this framework. However, this generalization leads to a higher numerical complexity. This can be seen by comparing the Hessian (49) to the Hessian defined by Eqs. (69)-(75). For instance, only the Hessian depending on pseudo stresses requires the third derivative of the yield function. In summary, the more general algorithm based on the pseudo stresses is thus numerically less efficient. Certainly, this is not surprising.

However, a more serious issue is related to the numerical stability of the algorithm discussed in the present subsection. More precisely, if Newton's method is applied, the Hessian matrix is highly ill-conditioned. Therefore, numerical problems occurred, even when a solver for indefinite matrices was employed. A careful analysis reveals different main sources for this pathological response. The first of those is related to the yield function. Since this function is positively homogeneous of degree one,

$$\left.\frac{\partial \phi}{\partial \boldsymbol{\Sigma}}\right|_{\boldsymbol{\Sigma}=\tilde{\boldsymbol{\Sigma}}} = \left.\frac{\partial \phi}{\partial \boldsymbol{\Sigma}}\right|_{\boldsymbol{\Sigma}=c\tilde{\boldsymbol{\Sigma}}} \qquad \forall c \in \mathbb{R}^+ \tag{78}$$

holds. Accordingly, the energy I_{inc} is invariant with respect to pseudo stresses being parallel to each other, i.e.

$$I_{\text{inc}}(\boldsymbol{F}_{n+1}, \Delta\lambda, \tilde{\boldsymbol{\Sigma}}) = I_{\text{inc}}(\boldsymbol{F}_{n+1}, \Delta\lambda, c\,\tilde{\boldsymbol{\Sigma}}) \qquad \forall c \in \mathbb{R}^+. \tag{79}$$

An additional source for the singularity of the Hessian matrix is associated with the space implicitly induced by the yield function. More specifically, the energy I_{inc} is constant for variations of the pseudo stresses in the direction of the kernel (denoted as "ker") of the projection operator $\mathbb{P}$ (see Eq. (35)). This property can be written as

$$I_{\text{inc}}(\boldsymbol{F}_{n+1}, \Delta\lambda, \tilde{\boldsymbol{\Sigma}}) = I_{\text{inc}}(\boldsymbol{F}_{n+1}, \Delta\lambda, \tilde{\boldsymbol{\Sigma}} + \boldsymbol{A}) \qquad \forall \boldsymbol{A} \in \ker(\mathbb{P}). \tag{80}$$

For instance, if a von Mises function is considered $\partial\phi/\partial\boldsymbol{\Sigma} = \operatorname{dev}\boldsymbol{\Sigma}/||\operatorname{dev}\boldsymbol{\Sigma}||$,

$$\frac{\operatorname{dev}\tilde{\boldsymbol{\Sigma}}}{||\operatorname{dev}\tilde{\boldsymbol{\Sigma}}||} = \frac{\operatorname{dev}\left[\tilde{\boldsymbol{\Sigma}} + \boldsymbol{A}\right]}{||\operatorname{dev}\left[\tilde{\boldsymbol{\Sigma}} + \boldsymbol{A}\right]||} \qquad \forall \boldsymbol{A} \in \ker(\mathbb{P}) = \{\mathbf{1}\; c \mid \forall c \in \mathbb{R}^+\}. \tag{81}$$

The final and probably least important issue concerning a parameterization depending on pseudo stresses is the symmetry of the flow rule in case of an elastically isotropic material model. Clearly, this problem could be solved by a projection method or by enforcing the respective constraints directly.

5 A numerically efficient variational constitutive update by means of a novel flow rule parameterization

In the present section, the aforementioned numerical problems associated with the variational constitutive update based on pseudo stresses are eliminated by combining the approach with another physically sound parameterization of the pseudo stresses. In this respect, the resulting algorithm can be understood as a multiple projection scheme.

5.1 Fundamentals

The singularity of the Hessian matrix due to the invariance of the energy I_{inc} with respect to the length of the pseudo stresses $\tilde{\boldsymbol{\Sigma}}$ can be simply eliminated by parameterizing the eigenvalues of $\tilde{\Sigma}_k$ by spherical coordinates (ψ,ρ). Thus, denoting the eigenprojection of $\tilde{\boldsymbol{\Sigma}}$ as $\boldsymbol{B}_k$, the representation

$$\tilde{\boldsymbol{\Sigma}} := \sum_{k=1}^{3} \tilde{\Sigma}_k(\psi, \rho)\; \boldsymbol{B}_k \tag{82}$$

with the eigenvalues

$$\tilde{\Sigma}_1 = \sin\psi\cos\rho, \quad \tilde{\Sigma}_2 = \sin\psi\sin\rho, \quad \tilde{\Sigma}_3 = \cos\psi \tag{83}$$

is considered in what follows. By using the parameterization (83) the constraint $||\tilde{\boldsymbol{\Sigma}}|| = 1$ is automatically fulfilled. For the sake of simplicity, three different eigenvalues are assumed here. Introducing the eigenprojections $\boldsymbol{B}_k^{\text{trial}}$ of the Mandel trial stresses, the tensors $\boldsymbol{B}_k$ can be obtained by an unknown rotation tensor $\boldsymbol{R}$. More explicitly and not enforcing a symmetric flow rule,

$$\boldsymbol{B}_k(\varphi_1, \vartheta_1, \chi_1, \varphi_2, \vartheta_2, \chi_2) = \boldsymbol{R}(\varphi_1, \vartheta_1, \chi_1) \cdot \boldsymbol{B}_k^{\text{trial}} \cdot \boldsymbol{R}^T(\varphi_2, \vartheta_2, \chi_2) \tag{84}$$

where the rotation tensor $\boldsymbol{R}$ is defined in standard manner as

$$\boldsymbol{R}(\varphi, \vartheta, \chi) = \boldsymbol{R}_1(\varphi) \cdot \boldsymbol{R}_2(\vartheta) \cdot \boldsymbol{R}_3(\chi) \tag{85}$$

with

$$\boldsymbol{R}_1(\varphi) := \begin{pmatrix} 1 & 0 & 0 \\ 0 & \cos\varphi & \sin\varphi \\ 0 & -\sin\varphi & \cos\varphi \end{pmatrix} \tag{86}$$

$$\boldsymbol{R}_2(\vartheta) := \begin{pmatrix} \cos\vartheta & 0 & -\sin\vartheta \\ 0 & 1 & 0 \\ \sin\vartheta & 0 & \cos\vartheta \end{pmatrix} \tag{87}$$

$$\boldsymbol{R}_3(\chi) := \begin{pmatrix} \cos\chi & \sin\chi & 0 \\ -\sin\chi & \cos\chi & 0 \\ 0 & 0 & 1 \end{pmatrix}. \tag{88}$$

If $(\varphi, \vartheta, \chi) = (0, 0, 0)$, the rotation tensor $\boldsymbol{R}$ equals the identity tensor and hence, $\boldsymbol{B}_k = \boldsymbol{B}_k^{\text{trial}}$. This is precisely the initial value of those angles in the resulting Newton iteration. In summary, the pseudo stresses are parameterized by means of the eight-dimensional representation

$$\tilde{\boldsymbol{\Sigma}}(\psi, \rho, \varphi_1, \vartheta_1, \chi_1, \varphi_2, \vartheta_2, \chi_2) = \boldsymbol{R}(\varphi_1, \vartheta_1, \chi_1) \cdot \left[\sum_{k=1}^{3} \tilde{\Sigma}_k(\psi, \rho)\ \boldsymbol{B}_k^{\text{trial}} \right] \cdot \boldsymbol{R}^T(\varphi_2, \vartheta_2, \chi_2). \tag{89}$$

Clearly, for elastically isotropic material models, the Mandel stresses and their pseudo counterparts are symmetric. In this case, Eq. (89) has to be replaced by the five-dimensional parameterization

$$\tilde{\boldsymbol{\Sigma}}(\psi, \rho, \varphi, \vartheta, \chi) = \boldsymbol{R}(\varphi, \vartheta, \chi) \cdot \left[\sum_{k=1}^{3} \tilde{\Sigma}_k(\psi, \rho)\ \boldsymbol{B}_k^{\text{trial}} \right] \cdot \boldsymbol{R}^T(\varphi, \vartheta, \chi). \tag{90}$$

If the yield function is also isotropic resulting in the coaxiality between the elastic right Cauchy-Green trial strains $\boldsymbol{C}^{\text{e trial}}$ and the Mandel stresses $\boldsymbol{\Sigma}$, the identity $\boldsymbol{B}_k = \boldsymbol{B}_k^{\text{trial}}$ holds. Accordingly, Eq. (90) can then be further simplified yielding

$$\tilde{\boldsymbol{\Sigma}}(\psi, \rho) = \sum_{k=1}^{3} \tilde{\Sigma}_k(\psi, \rho)\ \boldsymbol{B}_k^{\text{trial}}. \tag{91}$$

Consequently, if the model is fully isotropic (Ψ^{e} as well as ϕ), only two unknowns are required for spanning all admissible flow directions. Thus, the overall minimization problem depends on the three unknowns $\Delta\lambda, \psi, \rho$. It bears emphasis that the classical return-mapping in principal axes depends on four unknowns, cf. [1]. As a result, the proposed variational constitutive update is numerically even more efficient than the return-mapping scheme in this case. Furthermore and in line with this by now standard scheme, the numerically expensive tensorial derivatives of the exponential mapping (see [31]) can be avoided, since the eigenprojections are constant within the local stress update. For this reason, the variational constitutive update for fully isotropic constitutive models is highly efficient.

Besides the already discussed constraints included in the parameterizations (89)-(91), some yield functions induce an additional invariance within the energy I_{inc} (see Eq. (80)) and thus, they lead to an ill-conditioned Hessian matrix, if no further stabilization technique is used. One of the probably most practically relevant sources for such a singularity is concerned with the decomposition of the stress tensor into purely deviatoric and purely volumetric parts (see Eq. (81)). This is, for instance, relevant for von Mises- or Hill-type yield functions which are frequently employed in numerical simulations.

For a yield function (or some parts of that) only depending on the deviator $\operatorname{dev}\boldsymbol{\Sigma}$, the resulting flow rule is traceless, i.e. $\mathbf{1} : \partial_{\boldsymbol{\Sigma}}\phi = 0$. Considering the parameterization (89), this constraint requires

$$\sum_{k=1}^{3} \tilde{\Sigma}_k = 0. \tag{92}$$

Solving the characteristic polynomial of the stress tensor by means of Cardano's method with respect to the constraint Eq. (92) yields the parameterization

$$\tilde{\Sigma}_k(\psi) = \sqrt{\frac{2}{3}}\ \sin\left[\frac{2}{3}\,\pi\,k - \psi\right], \qquad k = \{1,2,3\}. \tag{93}$$

This parameterization will be used in the numerical examples presented in Section 6. According to Eq. (93), the respective implementation of the variational constitutive update for fully isotropic constitutive models depends only on the two unknowns $\Delta\lambda$ and ψ and therefore, it is numerically very efficient – even compared to the return-mapping scheme which requires a description depending on four unknowns in this case (using a Hencky model for Ψ^{e}, both algorithms can be reduced to scalar-valued equations, cf. [1, 3]).

Consistency of the algorithm

$$\begin{aligned}(\Delta\lambda, \boldsymbol{\Gamma}) = \arg\inf_{\Delta\lambda,\boldsymbol{\Gamma}} I_{\mathrm{inc}}|_{\boldsymbol{F}_{n+1}=\mathrm{const}}, \qquad \boldsymbol{P} = \partial_{\boldsymbol{F}_{n+1}} \inf_{\Delta\lambda,\boldsymbol{\Gamma}} I_{\mathrm{inc}} \\ I_{\mathrm{inc}} = \Psi_{n+1}(\boldsymbol{F}_{n+1}, \Delta\lambda, \boldsymbol{\Gamma}) - \Psi_n + \Delta\lambda\, Q_0^{\mathrm{eq}}.\end{aligned} \tag{94}$$

can be proved in a straightforward manner. Here and henceforth, $\boldsymbol{\Gamma}$ is the collection of all angles defining the respective parameterization. Thus, $\boldsymbol{\Gamma}$ is an eight-dimensional vector in the general case (see Eq. (89)), while it is one-dimensional for a fully isotropic constitutive model based on a von Mises yield function (see Eq. (93)). For distinguishing between the energy in Eq. (94) and that in Eq. (60), a superposed tilde sign is used for the parameterization depending directly on pseudo stresses (Eq. (60)). Denoting the composition of two functions in standard manner by $\circ$, the two different variational constitutive updates can be written as

$$I_{\mathrm{inc}} = \tilde{I}_{\mathrm{inc}} \circ \tilde{\mathbb{P}} \tag{95}$$

with

$$\begin{array}{rcccc} \tilde{\mathbb{P}} & : & (\mathbb{R}^{3\times3}, \mathbb{R}^{+}, \mathbb{R}^{8}) & \to & (\mathbb{R}^{3\times3}, \mathbb{R}^{+}, \mathbb{R}^{3\times3}) \\ & & (\boldsymbol{F}_{n+1}, \Delta\lambda, \boldsymbol{\Gamma}) & \mapsto & (\boldsymbol{F}_{n+1}, \Delta\lambda, \tilde{\boldsymbol{\Sigma}}). \end{array} \tag{96}$$

Therefore, the original structure is not affected by the novel parameterization and thus, the algorithm is consistent as well. This can be explicitly seen by analyzing the gradient of I_{inc} which is multiplicatively decomposed into the gradient of $\tilde{I}_{\mathrm{inc}}$ and the gradient of the parameterization $\tilde{\mathbb{P}}$.

5.2 Numerical implementation

5.2.1 The general case

In the general, not fully isotropic case, the unknown flow direction is either parameterized by the eight-dimensional representation (see Eq. (89)) or by the five-dimensional representation (see Eq. (90)). Independent of the considered case, all unknowns defining the flow direction are collected in the vector $\boldsymbol{\Gamma}$. Thus, the incremental energy is assumed to be of the type $I_{\mathrm{inc}} = I_{\mathrm{inc}}(\boldsymbol{F}_{n+1}, \Delta\lambda, \boldsymbol{\Gamma})$ in what follows. The resulting stress update algorithm (94) is effectively solved by a Newton-Raphson scheme. In this connection, the residual is introduced as

$$\boldsymbol{R}_{\mathrm{Newton}}(\Delta\lambda, \boldsymbol{\Gamma}) = [\boldsymbol{R}_{\Delta\lambda}(\Delta\lambda, \boldsymbol{\Gamma}); \boldsymbol{R}_{\boldsymbol{\Gamma}}(\Delta\lambda, \boldsymbol{\Gamma})] \tag{97}$$

with

$$\boldsymbol{R}_{\Delta\lambda}(\Delta\lambda, \tilde{\boldsymbol{\Sigma}}) = \frac{\partial I_{\mathrm{inc}}}{\partial \Delta\lambda} = \text{Eq. (62)} \tag{98}$$

$$\boldsymbol{R}_{\boldsymbol{\Gamma}}(\Delta\lambda, \tilde{\boldsymbol{\Sigma}}) = \frac{\partial I_{\mathrm{inc}}}{\partial \boldsymbol{\Gamma}} = \underbrace{\frac{\partial I_{\mathrm{inc}}}{\partial \tilde{\boldsymbol{\Sigma}}}}_{=\,\text{Eq. (63)}} : \frac{\partial \tilde{\boldsymbol{\Sigma}}}{\partial \boldsymbol{\Gamma}}. \tag{99}$$

Clearly, the gradient with respect to the plastic multiplier is not affected by the parameterization of the pseudo stresses and thus, it is equivalent to that previously derived. Furthermore and in line with the composition (95), residual (99) corresponding to the flow direction is multiplicatively decomposed into the gradient with respect to the pseudo stresses and the additional parameterization. This additional nonlinear projection is precisely the reason why the resulting scheme is numerically very stable.

The second derivatives of I_{inc} necessary for a Newton-Raphson scheme can be computed in a straightforward fashion. They result in

$$\frac{\partial^2 I_{\text{inc}}}{\partial \Delta\lambda^2} = \text{Eq. (69)} \tag{100}$$

$$\frac{\partial^2 I_{\text{inc}}}{\partial \boldsymbol{\Gamma}^2} = \left[\frac{\partial \tilde{\boldsymbol{\Sigma}}}{\partial \boldsymbol{\Gamma}}\right]^T : \underbrace{\frac{\partial^2 I_{\text{inc}}}{\partial \tilde{\boldsymbol{\Sigma}}^2}}_{=\text{Eq. (71)}} : \frac{\partial \tilde{\boldsymbol{\Sigma}}}{\partial \boldsymbol{\Gamma}} + \underbrace{\frac{\partial I_{\text{inc}}}{\partial \tilde{\boldsymbol{\Sigma}}}}_{=\text{Eq. (63)}} : \frac{\partial^2 \tilde{\boldsymbol{\Sigma}}}{\partial \boldsymbol{\Gamma}^2} \tag{101}$$

$$\frac{\partial^2 I_{\text{inc}}}{\partial \Delta\lambda\, \partial \boldsymbol{\Gamma}} = \underbrace{\frac{\partial^2 I_{\text{inc}}}{\partial \Delta\lambda\, \partial \tilde{\boldsymbol{\Sigma}}}}_{=\text{Eq. (70)}} : \frac{\partial \tilde{\boldsymbol{\Sigma}}}{\partial \boldsymbol{\Gamma}}. \tag{102}$$

Finally, if a certain convergence criterion is met within the iterative algorithm, the tangent moduli required for a Newton-Raphson algorithm at the structural level can be computed as

$$\frac{\mathrm{d}\boldsymbol{P}_{n+1}}{\mathrm{d}\boldsymbol{F}_{n+1}} = \frac{\partial^2 I_{\text{inc}}}{\partial \boldsymbol{F}_{n+1}^2} + \underbrace{\frac{\partial^2 I_{\text{inc}}}{\partial \boldsymbol{F}_{n+1} \partial \Delta\lambda}}_{=\text{Eq. (76)}} \otimes \frac{\mathrm{d}\Delta\lambda}{\mathrm{d}\boldsymbol{F}_{n+1}} + \underbrace{\frac{\partial^2 I_{\text{inc}}}{\partial \boldsymbol{F}_{n+1} \partial \tilde{\boldsymbol{\Sigma}}}}_{=\text{Eq. (77)}} : \frac{\partial \tilde{\boldsymbol{\Sigma}}}{\partial \boldsymbol{\Gamma}} : \frac{\mathrm{d}\boldsymbol{\Gamma}}{\mathrm{d}\boldsymbol{F}_{n+1}}. \tag{103}$$

The linearizations $\mathrm{d}\Delta\lambda/\mathrm{d}\boldsymbol{F}_{n+1}$ and $\mathrm{d}\boldsymbol{\Gamma}/\mathrm{d}\boldsymbol{F}_{n+1}$ in Eq. (103) follow again from linearizing the converged residual (97) with respect to $\Delta\lambda$, $\boldsymbol{\Gamma}$ and $\boldsymbol{F}_{n+1}$. Since this procedure has already been discussed in detail in Subsection 4.2.2 (see Eq. (53)), further details are omitted here.

5.2.2 Models based on an elastically isotropic response and an isotropic yield function

In case of an elastically isotropic response combined with an isotropic yield function, the trial elastic right Cauchy-Green tensor is coaxial to its converged counterpart which is in turn coaxial to the converged Mandel stresses. The eigenprojection of those tensors are again denoted as $\boldsymbol{B}_k$ and for the sake of simplicity three different eigenvalues are assumed. However, the more general case does not raise any additional problem and has been accounted for within the final implementation.

With the aforementioned assumptions, the exponential mapping involved in the time integration of $\boldsymbol{F}^{\text{p}}$ (see Eq. (27) and [31]) simplifies to

$$\exp\left[\Delta\lambda \;\; \partial_{\boldsymbol{\Sigma}}|_{\boldsymbol{\Sigma}=\tilde{\boldsymbol{\Sigma}}}\, \phi\right] = \sum_{k=1}^{3} \exp\left[\Delta\lambda \;\; \partial_{\Sigma_k}\phi|_{\Sigma_k=\tilde{\Sigma}_k}\right] \;\; \boldsymbol{B}_k \tag{104}$$

and accordingly, the elastic right Cauchy-Green strain tensor is given by

$$\boldsymbol{C}^{\text{e}}_{n+1} := \boldsymbol{F}^{\text{e}\,T}_{n+1} \cdot \boldsymbol{F}^{\text{e}}_{n+1} = \sum_{k=1}^{3} \lambda_k^{\boldsymbol{C}^{\text{e trial}}} \;\; \exp\left[-2\;\Delta\lambda \;\; \partial_{\Sigma_k}\phi|_{\Sigma_k=\tilde{\Sigma}_k}\right] \;\; \boldsymbol{B}_k. \tag{105}$$

Details concerning the exponetial mapping formulated in eigenvalues can be found in [31]. Here, $\lambda_k^{\boldsymbol{C}^{\text{e trial}}}$ are the eigenvalues of the elastic right Cauchy-Green tensor corresponding to the trial state. Since an elastically isotropic response is assumed, only the eigenvalues of $\boldsymbol{C}^{\text{e}}_{n+1}$ enter the stored energy potential. As implied by Eq. (105), such eigenvalues can be written as

$$\lambda_k^{\boldsymbol{C}^{\text{e}}} = \lambda_k^{\boldsymbol{C}^{\text{e trial}}} \;\; \exp\left[-2\;\Delta\lambda \;\; \partial_{\Sigma_k}\phi|_{\Sigma_k=\tilde{\Sigma}_k}\right]. \tag{106}$$

They depend on the plastic multiplier as well as on the parameterization of the eigenvalues $\tilde{\Sigma}_i$. Consequently, the resulting minimization problem reads

$$\inf I_{\text{inc}} \qquad \text{with} \qquad I_{\text{inc}}(\boldsymbol{F}_{n+1}, \Delta\lambda, \boldsymbol{\Gamma}) = \Psi_{n+1}(\boldsymbol{F}_{n+1}, \Delta\lambda, \boldsymbol{\Gamma}) - \Psi_n + \Delta\lambda\, Q_0^{\text{eq}} \tag{107}$$

where

$$\boldsymbol{\Gamma} = [\psi, \rho] \tag{108}$$

is two-dimensional in the more general case (see Eq. (82)), while it is one-dimensional for yield functions based on a volumetric/deviatoric decomposition of the stress tensor (see Eq. (93)), i.e.

$$\boldsymbol{\Gamma} = [\psi]. \tag{109}$$

As a result, the local stress update is based on a three- or two-dimensional optimization problem. Furthermore, the numerically expensive tensorial exponential mapping does not need to be computed. Consequently, the final algorithm is highly efficient. It bears emphasis that except for special cases, the return-mapping scheme for fully isotropic constitutive models requires the computation of four unknowns and is thus, often numerically more expensive.

Within the implementation, minimization problem $\inf_{\Delta\lambda,\mathbf{\Gamma}} I_{\text{inc}}$ has again been solved by a Newton-Raphson iteration and the consistent tangent moduli have been used at the structural level. Since the steps necessary for the respective derivations are identical to those already previously explained, further details are omitted here. A summary of the algorithm can be found in the appendix of the present paper.

6 Numerical examples

The performance of the proposed variational constitutive update is analyzed here. While the accuracy as well as the numerical efficiency of the stress update algorithm are discussed in Subsection 6.1 by means of a study at the material point level, a more complex boundary value problem is considered in Subsection 6.2.

6.1 Accuracy and performance analysis of the proposed variational constitutive update

For numerically analyzing the accuracy and the stability of the advocated variational constitutive updates, the concept of iso-error maps is employed, cf. [1, 2, 32–34]. Accordingly, a certain material point is considered and the stresses $\mathbf{\Sigma}$ are computed for different loading paths and different load step sizes (strain-controlled). By comparing the results to the analytical solution $\mathbf{\Sigma}_0$ (sufficiently small load steps), the error δ can be calculated. In this connection, this error is defined as

$$\delta = \frac{\sqrt{(\mathbf{\Sigma} - \mathbf{\Sigma}_0) : (\mathbf{\Sigma} - \mathbf{\Sigma}_0)}}{\sqrt{\mathbf{\Sigma}_0 : \mathbf{\Sigma}_0}} \cdot 100\,\%. \tag{110}$$

Within the current analysis, a fully isotropic constitutive model is adopted. While the elastic response is captured by a standard neo-Hooke-type law (Lamé constants λ and μ), plastic effects are accounted for by a von Mises yield function without hardening. The material parameters used within the numerical analyses are summarized in Tab. 1.

λ [kN/cm^2]	μ [kN/cm^2]	Q_0^{eq} [kN/cm^2]
67.27	81	$\sqrt{\frac{2}{3}}\,0.10$

Table 1: Material parameter defining the elastoplastic response. The Lamé constants λ and μ define the neo-Hooke-type energy for the elastic response, while Q_0^{eq} represents the initial yield stress.

The computed iso-error maps are illustrated in Figs. 1-3. As can be seen, the novel variational constitutive update (left hand side in Figs. 1-3) and the return-mapping scheme (right hand side in Figs. 1-3) show the same accuracy. This is not very surprising, since both methods rely on first-order accurate time integration schemes. It bears emphasis that in contrast to the variational constitutive update formulated in eigenvalues, the employed return-mapping scheme does not take advantage of the isotropy of the underlying constitutive model. For that purpose, the example was re-analyzed by using the variational constitutive update without considering the material symmetry. The respective results, not explicitly shown here, look identical to those of the implementation based on eigenvalues. For this reason, they have not been included in the paper.

Having discussed the accuracy of the method, focus is now on the numerical efficiency. The computing times necessary for different stress-update algorithms are summarized in Tab. 2. For every load case, the times are normalized with respect to that of the return-mapping scheme. Regarding the variational constitutive update, two different implementations are considered. The first of those does not take advantage of the material symmetry. It has been discussed in detail in Subsection 4.2. The second is an optimized code for fully isotropic models showing a deviatoric-type yield function and has been presented in Subsection 5.2.2. According to Tab. 2, the computational time of the standard parameterization is comparable to that of the classical return-mapping scheme. It bears emphasis that the computational

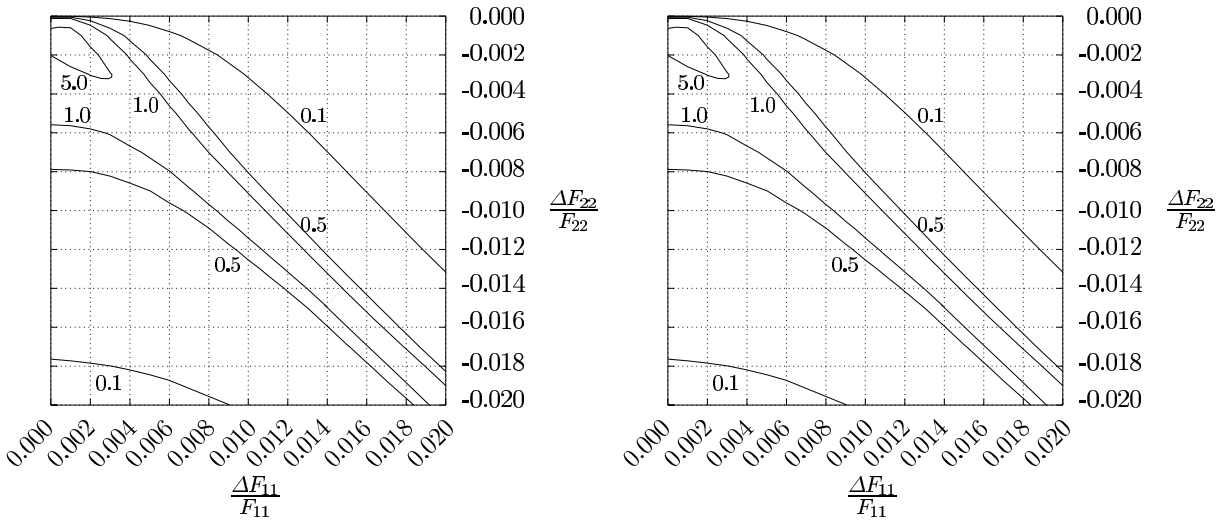

Figure 1: Iso-error maps for the fully isotropic von Mises plasticity model. Load case: uniaxial tension. Left hand side: error implied by the variational constitutive update based on a parameterization in terms of $(\Delta\lambda, \psi)$ (see Eq. (107) and Eq. (109)). Right hand side: error corresponding to a classical return-mapping scheme

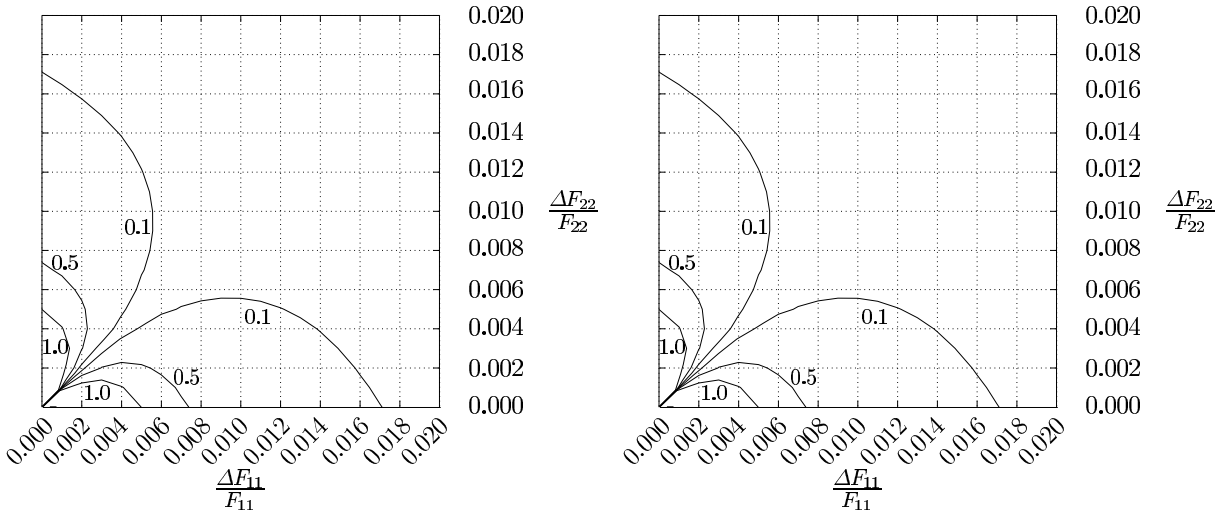

Figure 2: Iso-error maps for the fully isotropic von Mises plasticity model. Load case: biaxial tension. Left hand side: error implied by the variational constitutive update based on a parameterization in terms of $(\Delta\lambda, \psi)$ (see Eq. (107) and Eq. (109)). Right hand side: error corresponding to a classical return-mapping scheme

Load case	return-mapping scheme unknowns $\Delta\lambda$, $\boldsymbol{F}^{\mathrm{p}}$	variational constitutive update	
		standard formulation	eigenvalues
Simple tension	100 %	108 %	12 %
Biaxial tension	100 %	110 %	14 %
Pure shear	100 %	61 %	8 %

Table 2: Numerical efficiency of different stress update algorithms for the fully isotropic von Mises plasticity model without hardening. The computing time for every load case is related to that of the return-mapping scheme (100 %).

times depend strongly on the calculation of $\exp(\bullet)$, $\mathrm{Dexp}(\bullet)$ and $\mathrm{D}^2\exp(\bullet)$. In this connection, a method based on the spectral decomposition was significantly more efficient than that relying on a Taylor series, cf. [31]. If the material symmetry is accounted for, the complexity of the numerical scheme can be reduced

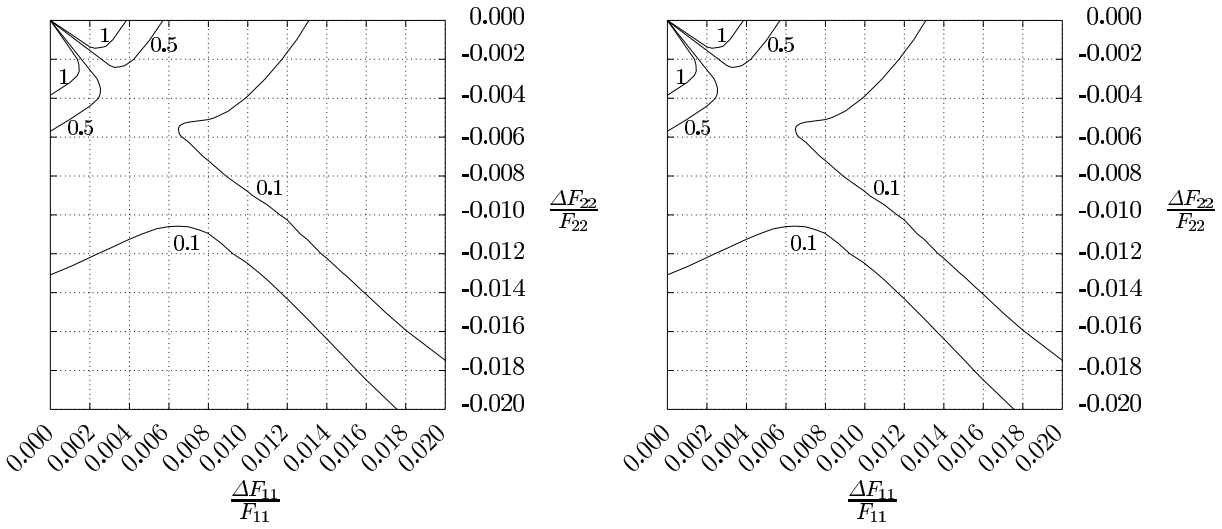

Figure 3: Iso-error maps for the fully isotropic von Mises plasticity model. Load case: pure shear. Left hand side: error implied by the variational constitutive update based on a parameterization in terms of $(\Delta\lambda, \psi)$ (see Eq. (107) and Eq. (109)). Right hand side: error corresponding to a classical return-mapping scheme

significantly resulting in an highly efficient implementation. As shown in Tab. 2, the respective computing times are thus considerably smaller.

6.2 A strip with a hole

Next, a more complex boundary value problem is numerically analyzed. The mechanical system depicted in Fig. 4 represents a standard benchmark, cf. [2, 35]. In line with [2, 35] the elastoplastic response of

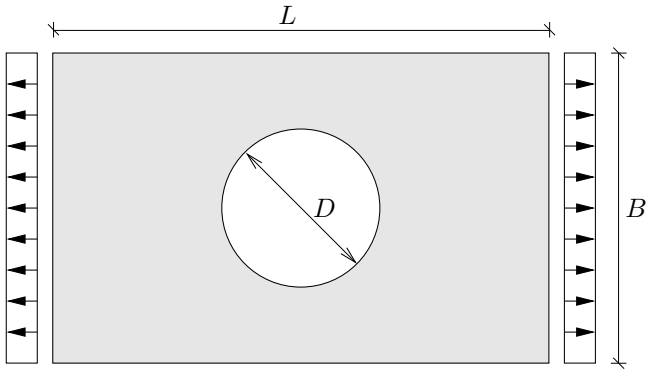

Geometry [cm]:		
L	36	
B	20	
D	10	
t	1.0	
Material parameters:		
E	70	kN/cm^2
ν	0.2	-
Q_0^{eq}	$\sqrt{2/3}$ 0.242	kN/cm^2
H_{i}	$\sqrt{2/3}$ 0.2	kN/cm^2

Figure 4: Strip with a circular hole: geometry, boundary conditions and material parameters. t denotes the thickness of the strip.

the strip with hole is modeled by means of an isotropic neo-Hooke-type model for the elastic response and an isotropic von Mises yield function with associative evolution equations for plastic deformation. Hardening is accounted for by an isotropic model with constant hardening modulus H_{i}. The numerical computations have been performed in a displacement-controlled manner.

The mechanical response predicted by the variational constitutive update is summarized in Fig. 5. As expected, the plastic deformation is large and localized in the vicinity of the hole. The remaining part of the structure deforms mostly elastically. The contour plot in Fig. 5 is in good agreement with the results previously reported in [6]. The same holds also for the load-displacement diagram. In line with [6] a softening behavior can be observed, although isotropic hardening is accounted for. Therefore, this softening is due to geometrical effects. Since the results of all different variational constitutive updates are identical, only those based on a direct parameterization of the flow rule are shown here (see Subsection 4.2). Furthermore, a difference between the accuracy of the return-mapping scheme and the variational constitutive update cannot be seen. However, it bears emphasis that particularly for highly

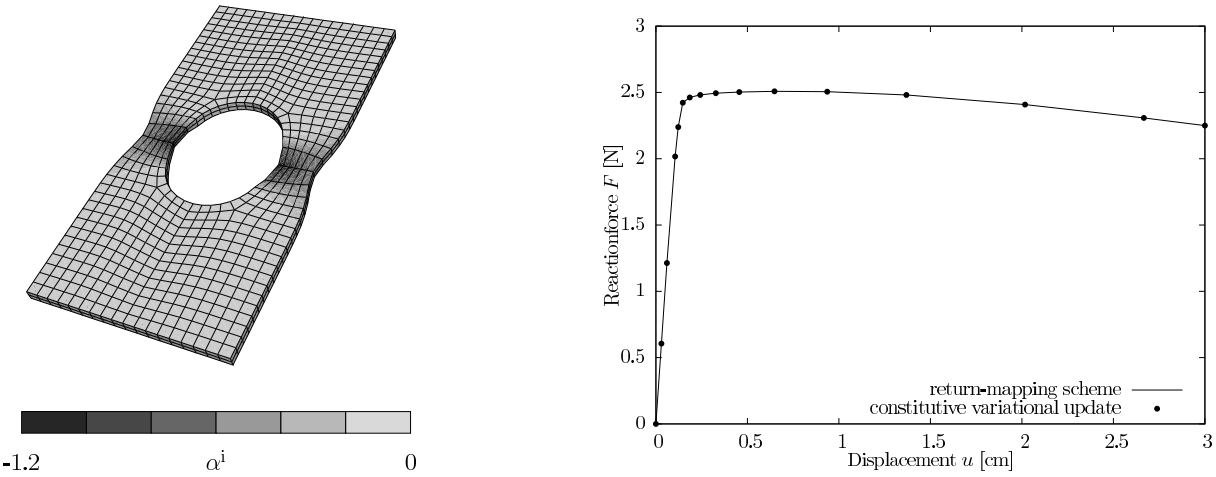

Figure 5: Strip with a circular hole: mechanical response as predicted by the novel variational constitutive update. The spatial discretization consists of 8-node tri-linear standard finite elements. Left hand side: distribution of the internal variable α_{i} corresponding to isotropic hardening; right hand side: load-displacement diagram

nonlinear problems, the variationally consistent method shows several significant advantages compared to the conventional return-mapping scheme. One such advantage is associated with effective line search strategies. More precisely, since the variational constitutive update is based on energy minimization, the considered numerical implementation possesses a natural process direction.

7 Conclusions

In the present paper, a novel implementation for variational constitutive updates has been advocated. The resulting scheme allows computing all state variables of a finite strain plasticity model naturally by minimizing the stress power of the considered solid. The presented framework is very general and can be applied to models showing an elastically anisotropic response, anisotropic yield functions as well as a combined isotropic, non-linear kinematic hardening behavior. For fully isotropic material models, an adapted algorithm has also been discussed. It is formulated in terms of eigenvalues and thus, it reduces the numerical complexity significantly and is highly efficient. More precisely, the respective algorithm depends on only three unknowns (two in case of purely deviatoric yield functions) and hence, it is even more efficient than a return-mapping scheme formulated in principal stress space which requires in each case one unknown more.

The development of the novel variational constitutive updates depended crucially on carefully analyzing different parameterizations of the flow rule. It turned out that a direct parameterization of the flow rule combined with a projection scheme is numerically stable. However, this projection scheme can only be applied to a relatively small family of yield function and thus, it narrows the range of application considerably. By way of contrast, a parameterization depending on the concept of pseudo stresses does not show this shortcoming. Unfortunately, an implementation of this method by using Newton's method led to an ill-conditioned Hessian matrix. This singularity could be effectively eliminated by means of an additional parameterization.

Numerical experiments indicated that the proposed variational constitutive update is at least as accurate as the conventional and well established return-mapping scheme. Furthermore, the novel stress update algorithm is highly efficient and in many cases even more efficient than the return-mapping scheme. Certainly, it has already been known that variational constitutive updates show several advantages compared to classical methods known from computational plasticity theory. However, in the present paper is was shown that the underlying variational structure can also be used for developing highly efficient numerical implementations. For this reason, the authors hope that this mathematically and physically elegant method will be applied more often in the future.

1. Compute trial state
   given: $\boldsymbol{F}_n^{\mathrm{p}}, \alpha_{\mathrm{i}}|_n, \boldsymbol{F}_{n+1}$
   compute trial strains: $\boldsymbol{F}_{n+1}^{\mathrm{trial}}$, $\boldsymbol{C}^{\mathrm{e\,trial}}$, $\lambda_k^{\boldsymbol{C}^{\mathrm{e\,trial}}}$, $\boldsymbol{B}_k^{\mathrm{trial}}$, see Eq. (105)
   compute trial stresses: $\boldsymbol{\Sigma}_{n+1}^{\mathrm{trial}}$, $\tilde{\boldsymbol{\Sigma}}^{\mathrm{trial}} = \boldsymbol{\Sigma}_{n+1}^{\mathrm{trial}}/||\boldsymbol{\Sigma}_{n+1}^{\mathrm{trial}}||$
   compute trial angles: ψ^{trial}, ρ^{trial}, see Eq. (83)

2. Set initial values
   $\psi_0 = \psi^{\mathrm{trial}}$, $\rho_0 = \rho^{\mathrm{trial}}$, $\Delta\lambda = 0$

3. UNTIL $||\boldsymbol{R}|| > \mathrm{tol}$ DO:

   (a) Compute gradient of incremental energy I_{inc} (residual) $\mathbf{R} := [R_{\Delta\lambda}; R_{\Delta\psi}; R_{\Delta\rho}]$

$$\mathbf{R}_{\Delta\lambda} = -2\sum_{k=1}^{3}\left\{\lambda_k^{\boldsymbol{C}^{\mathrm{e\,trial}}}\,\frac{\partial\Psi^{\mathrm{e}}}{\partial\lambda_k^{\boldsymbol{C}}}\,\exp\left[-2\,\Delta\lambda\,\partial_{\Sigma_k}\phi|_{\Sigma_k=\tilde{\Sigma}_k}\right]\,\partial_{\Sigma_k}\phi|_{\Sigma_k=\tilde{\Sigma}_k}\right\} + Q_{\mathrm{i}} + Q_0^{\mathrm{eq}}$$

$$\mathbf{R}_{\Delta\psi} = -2\,\Delta\lambda\sum_{k=1}^{3}\left\{\lambda_k^{\boldsymbol{C}^{\mathrm{e\,trial}}}\,\frac{\partial\Psi^{\mathrm{e}}}{\partial\lambda_k^{\boldsymbol{C}}}\,\exp\left[-2\,\Delta\lambda\,\partial_{\Sigma_k}\phi|_{\Sigma_k=\tilde{\Sigma}_k}\right]\,\partial^2_{\Sigma_k\psi}\phi\big|_{\Sigma_k=\tilde{\Sigma}_k}\right\}$$

$$\mathbf{R}_{\Delta\rho} = -2\,\Delta\lambda\sum_{k=1}^{3}\left\{\lambda_k^{\boldsymbol{C}^{\mathrm{e\,trial}}}\,\frac{\partial\Psi^{\mathrm{e}}}{\partial\lambda_k^{\boldsymbol{C}}}\,\exp\left[-2\,\Delta\lambda\,\partial_{\Sigma_k}\phi|_{\Sigma_k=\tilde{\Sigma}_k}\right]\,\partial^2_{\Sigma_k\rho}\phi\big|_{\Sigma_k=\tilde{\Sigma}_k}\right\}$$

   (b) Compute the Hessian matrix $\mathbb{H}$ of I_{inc}, i.e., the gradient of $\mathbf{R}$ with respect to $\Delta\lambda$, ρ and ψ

   (c) Update the unknowns $\boldsymbol{U} = [\psi; \rho, \Delta\lambda]$ (with or without line search, cf. [36])

$$\boldsymbol{U}_{n+1} = \boldsymbol{U}_n - \mathbb{H}^{-1}\cdot\boldsymbol{R}$$

4. Update of the deformation gradient $\boldsymbol{F}^{\mathrm{p}}$

$$\boldsymbol{F}_{n+1}^{\mathrm{p}} = \exp\left[\Delta\lambda\,\partial_{\boldsymbol{\Xi}}\phi|_{n+1}\right]\cdot\boldsymbol{F}_n^{\mathrm{p}}$$

5. Update of the stresses: $\boldsymbol{F}_{n+1}^{\mathrm{e}} = \boldsymbol{F}_{n+1}\cdot\boldsymbol{F}^{\mathrm{p}}{}_{n+1}^{-1}$, $\boldsymbol{S}_{n+1} = 2\,\boldsymbol{F}^{\mathrm{p}}{}_{n+1}^{-1}\cdot\dfrac{\partial I_{\mathrm{inc}}}{\partial\boldsymbol{C}^{\mathrm{e}}}\cdot\boldsymbol{F}^{\mathrm{p}}{}_{n+1}^{-T}$

Figure 6: Variational constitutive update for fully isotropic models briefly: stress update algorithm in principal axes. Loading is checked by the discrete loading condition $\phi^{\mathrm{trial}} > 0$.

A Variational Constitutive update in principal axes for fully isotropic models

In this appendix, the variational constitutive update for fully isotropic models briefly discussed in Subsection 5.2.2 is summarized. The resulting algorithm for the computation of the stresses is shown in Fig. 6. For deriving the consistent tangent moduli, the algorithm is first linearized for fixed principal axes. Subsequently, it is transformed to the general stress space. Since this procedure is nowadays standard and can be found, e.g. in [1], further details are omitted here.

References

[1] J.C. Simo. Numerical analysis of classical plasticity. In P.G. Ciarlet and J.J. Lions, editors, *Handbook for numerical analysis*, volume IV. Elsevier, Amsterdam, 1998.

[2] J.C. Simo and T.J.R. Hughes. *Computational Inelasticity*. Springer, New York, 1998.

[3] M. Ortiz and L. Stainier. The variational formulation of viscoplastic constitutive updates. *Computer Methods in Applied Mechanics and Engineering*, 171:419–444, 1999.

[4] M. Ortiz and E.A. Repetto. Nonconvex energy minimization and dislocation structures in ductile single crystals. *Journal of the Mechanics and Physics of Soils*, 47:397–462, 1999.

[5] K. Hackl and F. D. Fischer. On the relation between the principle of maximum dissipation and inelastic evolution given by dissipation potentials. *Proceeding of the Royal Society A*, 464:117–132, 2008.

[6] J. Mosler. Variationally consistent modeling of finite strain plasticity theory with non-linear kinematic hardening. *Computer Methods in Applied Mechanics and Engineering*, 199:2753–2764, 2010.

[7] C. Miehe, N. Apel, and M. Lambrecht. Anisotropic additive plasticity in the logarithmic strain space: modular kinematic formulation and implementation based on incremental minimization principles for standard materials. *Computer Methods in Applied Mechanics and Engineering*, 191, 2002.

[8] C. Carstensen, K. Hackl, and A. Mielke. Non-convex potentials and microstructures in finite-strain plasticity. *Proceedings of the Royal Society of London Series A*, 458(2018):299–317, 2002.

[9] H. Petryk. Incremental energy minimization in dissipative solids. *Comptes Rendus Mecanique*, 331:469–474, 2003.

[10] J. Mosler and O.T. Bruhns. On the implementation of rate-independent standard dissipative solids at finite strain – variational constitutive updates. *Computer Methods in Applied Mechanics and Engineering*, 9–12:417–429, 2009.

[11] J. Mosler and M. Ortiz. h-adaption in finite deformation elasticity and plasticity. *International Journal for Numerical Methods in Engineering*, 72:505–523, 2007.

[12] G.M. McNeice and P.V. Marcal. Optimization of finite-element grids based on minumum potential-energy. *Journal of Engineering for Industry-Transactions of the ASME*, 95(1):186–190, 1973.

[13] C. Felippa. Numerical experiments in finite element grid optimization by direct energy search. *Appl. Math. Modelling*, 1:93–96, 1976.

[14] J. Mosler and M. Ortiz. On the numerical implementation of variational arbitrary Lagrangian-Eulerian (VALE) formulations. *International Journal for Numerical Methods in Engineering*, 67:1272–1289, 2006.

[15] J. Mosler and M. Ortiz. An error-estimate-free and remapping-free variational mesh refinement and coarsening method for dissipative solids at finite strain. *International Journal for Numerical Methods in Engineering*, 77:437–450, 2009.

[16] J. Mosler and F. Cirak. A variational formulation for finite deformation wrinkling analysis of inelastic membranes. *Computer Methods in Applied Mechanics and Engineering*, 198:2087–2098, 2009.

[17] M. Homayonifar and J. Mosler. On the coupling of plastic slip and deformation-induced twinning in magnesium: A variationally consistent approach based on energy minimization. *International Journal of Plasticity*, 2010. in press.

[18] M. Canadija and J. Mosler. On the thermomechanical coupling in finite strain plasticity theory with non-linear kinematic hardening by means of incremental energy minimization. *International Journal of Solids and Structures*, 48:1120–1129, 2011.

[19] J. Mosler and O.T. Bruhns. Towards variational constitutive updates for non-associative plasticity models at finite strain: models based on a volumetric-deviatoric split. *International Journal of Solids and Structures*, 46:1676–1684, 2009.

[20] E.H. Lee. Elastic-plastic deformation at finite strains. *Journal of Applied Mechanics*, 36:1–6, 1969.

[21] J. Lubliner. *Plasticity Theory*. Maxwell Macmillan International Editions, 1997.

[22] B. Coleman and W. Noll. The thermodynamics of elastic materials with heat conduction and viscosity. *Archive for Rational Mechanics and Analysis*, 13:167–178, 1963.

[23] B. Coleman and M. Gurtin. Thermodynamics with internal state variables. *Journal of Chemical Physics*, 47:597–613, 1967.

[24] J. Mandel. *Plasticite classique et viscoplasticitite*. CISM, 1971.

[25] A.M. Maugin. *The Thermodynamics of Plasticity and Fracture*. Cambridge University Press, 1992.

[26] B. Halphen and Q.S. Nguyen. Sur les matériaux standards généralisés. *J. Méchanique*, 14:39–63, 1975.

[27] J. Lemaitre. A continuous damage mechanics model for ductile fracture. *J. Eng. Mat. Techn.*, 107:83–89, 1985.

[28] J. Lemaitre and J.-L. Chaboche. *Mechanics of Solid Materials*. Cambridge University Press, 1994.

[29] M. Wallin, M. Ristinmaa, and N.S. Ottosen. Kinematic hardening in large strain plasticity. *Eur. J. Mech. A/Solids*, 22:341–356, 2003.

[30] A. Menzel, M. Ekh, K. Runesson, and P. Steinmann. A framework for multiplicative elastoplasticity with kinematic hardening coupled to anisotropic damage. 21:371–434, 2005.

[31] M. Ortiz, R.A. Radovitzky, and E.A. Repetto. The computation of the exponential and logarithmic mappings and their first and second linearizations. *International Journal for Numerical Methods in Engineering*, 52:1434–1441, 2001.

[32] R.D. Krieg and D.B. Krieg. Accuracies of numerical simulation methods for the elastic-perfectly plastic model. *Journal of Pressure Vessel Technology*, 99:510–515, 1977.

[33] M. Ortiz and E.P. Popov. Accuracy and stability of integration algorithms for elastoplastic constitutive relations. *International Journal for Numerical Methods in Engineering*, 21:1561–1576, 1985.

[34] M. Ortiz and J.C. Simo. An analysis for a new class of integration algorithmus for elastoplastic constitutive relations. *International Journal for Numerical Methods in Engineering*, 23:353–366, 1986.

[35] P. Fuschi, D. Perić, and D.R.J. Owen. Studies on generalized midpoint integration in rate-independent plasticity with reference to plane stress J_2-flow theory. 43:1117–1133, 1992.

[36] C. Geiger and C. Kanzow. *Numerische Verfahren zur Lösung unrestringierter Optimierungsaufgaben*. Springer, New York, 1999.